JGR Oceans

RESEARCH ARTICLE
10.1029/2020JC016118

Key Points:

- This is a first attempt to generate analysis data based on a surface wave-tide-circulation fully coupled model system, First Institute of Oceanography Coupled Ocean Model
- The quality of this data set is comprehensively verified through comparison with two other analysis datasets and observations
- The new data set can well capture the seasonal variation of sea surface temperature, mixed layer depth, *El Niño*, Indian Ocean dipole, and Atlantic meridional mode

Correspondence to:
W. Perrie,
William.Perrie@dfo-mpo.gc.ca

Citation:
Sun, Y., Perrie, W., Qiao, F., & Wang, G. (2020). Intercomparisons of high-resolution global ocean analyses: Evaluation of a new synthesis in tropical oceans. *Journal of Geophysical Research: Oceans*, *125*, e2020JC016118. https://doi.org/10.1029/2020JC016118

Received 9 FEB 2020
Accepted 5 NOV 2020

Intercomparisons of High-Resolution Global Ocean Analyses: Evaluation of A New Synthesis in Tropical Oceans

Yujuan Sun[1,2,3], William Perrie[2], Fangli Qiao[1,4,5], and Gang Wang[1,4,5]

[1]First Institute of Oceanography, Ministry of Natural Resources, Qingdao, China, [2]Bedford Institute of Oceanography, Fisheries and Oceans Canada, Dartmouth, NS, Canada, [3]National Oceanography Centre, Liverpool, UK, [4]Laboratory for Regional Oceanography and Numerical Modeling, Pilot National Laboratory for Marine Science and Technology, Qingdao, China, [5]Key Laboratory of Marine Science and Numerical Modeling, Ministry of Natural Resources, Qingdao, China

Abstract A new high-resolution global analysis product is constructed from a fully coupled surface wave-tide-circulation Ocean Model developed by the First Institute of Oceanography Coupled Ocean Model (FIO-COM). The performance of the FIO-COM analysis data set is assessed based on comparisons with two other widely used high-resolution global analysis products (Copernicus marine and environment monitoring service and HYbrid isopycnal-sigma-pressure coordinate ocean model), and observations in tropical oceans. Through comparison with observations, the FIO-COM analysis is shown to be able to accurately capture the large-scale mixed layer depth (MLD) structures in the tropical oceans during all seasons. Seasonal variations of MLDs can exceed ±80% in the southern and northern tropical oceans (10°-25°S and 10°-25°N) in both boreal winter and summer, as inferred from observations and FIO-COM analysis data. Quantitative assessments of the 20°C isothermal depth, temperature at 5°m depth, and temperature and salinity profiles, among the analyses and in situ observations are also conducted. The capability of the FIO-COM analysis to reflect the observed sea surface temperature variability during the 2015 *El Niño* episode is further investigated through comparisons with observations from 19 TAO buoys located in the *Niño* 3.4 region. All indicate the high quality of the new data set.

Plain Language Summary We present a new high-resolution global analysis data set, which is for the first time constructed from a surface wave-tide-circulation fully coupled model system. To evaluate the accuracy of the analysis data set, we present intercomparisons with two other high-resolution global analysis datasets, as well as observations from tropical ocean areas. We show that the new analysis data set simulates the large-scale ocean mixed layer depth structures accurately during all seasons over a two-year period. Specifically, we make comparisons with in situ observations of the 20°C isothermal depth, temperature at 5°m depth, and the temperature and salinity profiles. The new data set exhibits high quality in all of these variables.

1. Introduction

Global ocean analyses not only describe the large-scale and long-term patterns of the global oceans, but also provide the basic information of the initial and boundary conditions for regional ocean model simulations. Generally, the analysis data can be described as a combination of ocean models and observations through data assimilation schemes. However, model resolution and computation costs constrain the development of these assimilative datasets. Dickey (2003) has demonstrated that the application of ocean observations, in the space-time continuum, in conjunction with ocean models with increased spatial and temporal resolution, are key elements to achieve increasing accuracy and efficacy in data assimilation. With the synergistic development of these observational and modeling activities, ocean data assimilation has shown an ability to provide daily output products with spatial resolutions as fine as 10 km; this is particularly well-suited to capture mesoscale phenomena (such as fronts, eddies, etc.). Compelling evidence can be found in recent studies showing the important impact of eddy-resolving ocean models on simulations of fronts, eddies, ocean circulations, and energy spectrum (Chin et al., 2017; Ignatov et al., 2016; Soufflet et al., 2016), which can even further influence the large-scale climate system (Kirtmsan et al., 2012; Scaife et al., 2011).

As model resolution has been getting increasingly higher, our ability to accurately simulate the mixed layer depth (MLD) in the upper ocean in ocean general circulation models remains a great challenge, especially because the simulated MLD is often too shallow in the summer time. As the MLD is a key factor in ocean dynamics, in typhoon/hurricane evolution studies and in climate change simulations, tremendous efforts have been made in the ocean community to address this problem. With this motivation, a Coupled surface wave-tide-circulation Ocean Model was developed by the First Institute of Oceanography (FIO-COM), based on nonbreaking surface wave-induced mixing as proposed by Qiao et al. (2004), which is also known as Qiao's model. Among studies that have been completed, the enhanced MLD simulation in FIO-COM, has been found to be among the best that have been put forward (Wu et al., 2015). This has provided a unique chance to build a new analysis data set that can accurately reproduce the ocean MLD properties, based on this coupled model system.

However, an essential priority is to assess the performance of the FIO-COM analysis data set before this product can be publically released to the oceanographic community. An intercomparison of the FIO-COM analysis data set and other high-resolution global analysis datasets is an effective and direct way to validate its accuracy, with respect to observations, including individual observations and monthly mean gridded observational datasets. The validation of the FIO-COM analysis data set can be divided into two parts. The first is to compare model results with individual observations, such as buoy data and in situ T/S profiles, and quantitatively assess the performance of the FIO-COM analysis data set with respect to T/S profiles, the 20°C isothermal depth (representing MLD) and temperatures at 5 m depth. The second is to compare FIO-COM analysis with a gridded observational data set. Because the MLD is not assimilated directly into the analysis datasets as an independent parameter, therefore, validation of MLD can be an index assessing FIO-COM's ability to reproduce the subsurface physical dynamic processes, in global analysis datasets.

The significance of the mixed layer is that it has a key role in the air-sea interactions, due to the large influence that it has on ocean surface heat fluxes (Foltz et al., 2003; Lee et al., 2015), because the specific heat of ocean water is 3,100 times larger than that of air. MLD variations can control global ocean climate variability, and global climate change will reflect MLD changes (Lee et al., 2015; Yeh et al., 2009). Monterey and Levitus (1997, p. 300) analyzed the climatological monthly mean maps of the global ocean MLDs, and concluded that there is strong MLD seasonality in mid and high latitudes. Their work also indicates that MLD changes between summer and winter are ∼10%–20% of the annual mean MLD in equatorial latitudes (10°S-10°N). However, they did not focus on investigating the MLD seasonality in the tropical oceans. Kara et al. (2003) presented monthly MLD climatological fields for the global ocean based on the World Ocean Atlas (1994), reporting strong MLD seasonality in the subtropical Pacific Ocean and higher latitudes; but they provided few details regarding the tropical oceans. Later, Carton et al. (2008) investigated the MLD variability based on the World Ocean Atlas 2005 global ocean data set. Their study tended to examine the interannual MLD variations on the global scale, but they also failed to describe the seasonal MLD cycle in the tropical oceans. Keerthi et al. (2013) expanded these studies to provide detailed investigations of the interannual MLD fluctuations for the tropical Indian Ocean and discussed the influences of the Indian Ocean dipole (IOD) and monsoon. More recently, Rugg et al. (2016) suggested that ocean mixed layer dynamics, that is, MLD changes, can significantly contribute to interannual variations of sea surface temperature (SST) in the tropical North Atlantic Ocean.

Previous studies and validations of MLD variations on the global scale are mostly based on analyses of averages or individual observation datasets (Cronin & Kessler, 2002; de Boyer Montégut et al., 2004), which are restricted by the scarcity of the observations in both spatial and temporal resolutions (Carton et al., 2008; de Boyer Montégut et al., 2004; Monterey & Levitus, 1997). Climatological datasets with relative coarse horizontal and vertical resolutions can capture the large-scale MLD features, but fail to provide accurate MLD estimates or to give detailed descriptions in regional areas. By contrast, the application of relatively accurate global analysis datasets to investigations of MLD variability can provide some compensation for this insufficiency. Toyoda et al. (2017) examined the MLD fields estimated from a suite of major ocean analyses datasets, with horizontal resolutions in the range of 1° to 1/4°, and they suggested that reduced bias is largely attributed to higher resolution. Here we use relatively high-resolution global ocean analysis datasets to estimate the MLDs over the tropical oceans within the latitudes between 25°S to 25°N, and we conduct intercomparisons of MLDs, with associated observational datasets. In addition, the seasonal variations of

MLDs are also investigated. We show that the nonbreaking surface wave-induced vertical mixing is important for reliable simulation of the MLD.

In this study, as a demonstration, the FIO-COM data set consists of two years, 2014 and the *El Niño* year 2015. The objective of this paper is to make preliminary validation of the data quality. A long period reanalysis data set is under construction and will be evaluated after it is deemed ready. In this regard, we denote our short term data set as an analysis data set. Section 2 describes the other two analysis datasets and the observational data used for the validation. Intercomparisons of seasonal MLDs estimated from the three analyses and the observations are presented in Section 3. Further assessments with individual observations, including the 20°C isothermal depth, the temperature at 5 m depth, and temperature and salinity profiles, are conducted in Section 4. The performance of the FIO-COM analysis in reproducing the SST variation during the strong 2015 *El Niño* episode is presented in Section 5. Sections 6 and 7 give the discussion and summary, respectively.

2. Model and Datasets

2.1. FIO-COM and Data Assimilation Scheme

With the enhanced intersection of new technologies in ocean modeling and soft and hardware innovations in computer science, the goal of building a high-resolution eddy-resolving global ocean model is achievable. Moreover, the development of corresponding high-resolution (~10 km) global ocean analysis datasets is now also within reach. A 0.1° × 0.1° global high-resolution analysis data set has recently been developed by the First Institute of Oceanography to meet the increasing application demands of the oceanographic community (http://fiocom.fio.org.cn/). The FIO-COM coupled model system includes the modular ocean model version 5 (MOM5) (Griffies, 2012), the third-generation MASNUM surface wave model (Qiao et al., 2016a), and the sea ice simulator (SIS) ice model (Winton, 2000). The horizontal resolution of FIO-COM is 0.1° × 0.1° with 54 vertical layers, varying from 2 m at the surface to 366 m at the bottom. The initial conditions were derived from the integral results of MOM5 forced by CORE2 (Version two forcing for coordinated ocean-ice reference experiments; Griffies et al., 2009). The atmospheric forcing was input into FIO-COM every 3 h, including the air temperature, atmospheric pressure on the sea surface, ocean surface wind at 10 m height, the precipitation, and specific humidity and heat flux, which were obtained from a weather forecast model of global forecast system (GFS) operated by the National centers for environmental prediction of USA (NCEP). For years 2014 and 2015, the model is forced by NCEP GFS 0.5° × 0.5° resolution data. From year 2016 onwards, NCEP GFS 0.25° × 0.25° fields are used (https://www.nco.ncep.noaa.gov/pmb/products/gfs/). The air-sea fluxes are calculated by using the CORE bulk formula (Large & Yeager, 2004), and wind-stress is not modulated by the wave states.

For the FIO-COM analysis data set, the most distinguishing feature is the implementation of the nonbreaking surface wave-induced mixing added to the K-profile parameterization (KPP) vertical mixing scheme in the ocean model (Qiao et al., 2004, 2008, 2016a). This formulation for wave-induced mixing can effectively alleviate the vertical mixing problem in the upper ocean which has been a bottleneck for nearly all ocean circulation models (Fan & Griffies, 2014; Shu et al., 2011; Wu et al., 2015). The nonbreaking surface wave-induced mixing is analytically expressed as

$$B_v = \alpha \iint_{\bar{k}} E\left(\bar{k}\right)\exp\left(2kz\right)\mathrm{d}\bar{k}\,\frac{\partial}{\partial z}\left[\iint_{\bar{k}} \omega^2 E\left(\bar{k}\right)\exp\left(2kz\right)\mathrm{d}\bar{k}\right]^{1/2} \tag{1}$$

where, $\bar{k}$ is wave number, ω is the wave angular frequency, z is vertical depth with $z = 0$ at the mean sea level, α is a coefficient which may be calibrated by observations, and can be set as 1.0 (Qiao et al., 2004). $E\left(\bar{k}\right)$ represents the wave number spectrum including both wind waves and swell waves. The wave-induced mixing term B_v term can be motivated physically by assuming that the surface waves can be approximated as monochromatic (Qiao et al., 2010), in which case B_v can be expressed as

$$B_v = \alpha A^3 k\omega \exp\left\{3kz\right\} = \alpha A u_s \exp\left\{3kz\right\} \tag{2}$$

where $u_s = c\,(Ak)^2$ is the Stokes drift, $c = \omega / k$ is the phase velocity of surface wave, and B_v is physically related to the Stokes drift. In this formulation, B_v is exchanged between the ocean circulation model and the surface wave model, daily.

Tide-induced mixing is also considered, due to its key role in the bottom layer and coastal areas (Lü et al., 2008). Tidal mixing is obtained from a global tide model including eight major tidal constituents (Xiao et al., 2016). An internal tide drag parameterization (Jayne & St. Laurent, 2001) is adopted in the global tide model to improve the accuracy of the simulated global tide in both deep and shallow areas.

The data assimilation scheme is based on the ensemble adjustment kalman filter (EAKF) method (Anderson, 2011), which has also been implemented in other ocean circulation models (Yin et al., 2011). The implementation consists of two steps (Yin et al., 2012). The first step is to calculate the departure of all the ensembles of assimilative variables (such as SST, temperature, salinity, and sea surface height), with respect to the observational data at observing locations. The second step is to calculate the increments for the assimilative variables, at model grid points, based on the covariance between ensembles at both model grids and observing locations, incorporated with the increments from the first step. The covariance between multiple variables are calculated, and the localization of covariance is performed by a polynomial function. The settings of Euclidean spatial distances in this function are different, such as for Argo temperature and salinity, it is selected as 2° horizontally, 100 m vertically, and 5 days in time (Yin et al., 2011). Here, the observational datasets assimilated into FIO-COM are limited, only including the optimally interpolated microwave and infrared SST observations (http://www.remss.com), maps of sea level anomalies (SLA) obtained from Ssalto/Duacs altimeter products produced by the Copernicus marine and environment monitoring service (CMEMS) and Argo Salinity and Temperature profiles. The FIO-COM analysis data set provides daily global ocean analysis data from January 1, 2014 to the present, including temperature, salinity, current velocity (U/V) and sea surface height.

FIO-COM is a first attempt to generate analysis data, based on a surface wave-tide-circulation coupled model system. The newly developed analysis data set reflects the additional mixing due to B_v. Thus, FIO-COM aims to mitigate the problem of insufficient mixing in the upper ocean that exists almost universally, in all ocean models especially in summer time.

2.2. HYCOM and CMEMS Analyses

Two other high-resolution global ocean analyses, both with horizontal resolutions of 1/12° × 1/12°, have been developed, and widely used so far. One is produced from the global data-assimilative HYbrid isopycnal-sigma-pressure coordinate ocean model (HYCOM; Bleck, 2002), developed as part of the USA Global ocean data assimilation experiment (GODAE), known as HYCOM analysis. The second one is produced by Mercator analysis and forecast operational system (PSY4QVSR1 GL12), provided by CMEMS, hereafter denoted as CMEMS analysis (or Mercator analysis).

The advantage of HYCOM analysis is the implementation of a substantially evolved hybrid vertical coordinate system, which remains isopycnic in the well-stratified open ocean and combines other different types of coordinates, transiting to level coordinates in less-stratified regions (surface mixed layer) and very shallow water, and to terrain-following sigma coordinates in nearshore regions (G. R. Halliwell, 2004; G. Halliwell et al., 1998). This feature gives HYCOM the ability to optimally simulate coastal and open ocean circulations. The Navy coupled ocean data assimilation (NCODA) system is employed for data assimilation in HYCOM, including remotely sensed SSTs, sea surface height, in situ surface and subsurface T/S profiles, and currents (Chassignet et al., 2007; Cummings, 2005; Cummings & Smedstad, 2013; Cummings & Smedstad, 2014). Here, we use the HYCOM + NCODA global 1/12° × 1/12° analysis data set (GLBu0.08), which are provided in a uniformly constant horizontal latitude/longitude grid, and 40 standard z-levels. Regarding HYCOM analysis, our main concern is that the interpolation to 40 standard z-levels might reduce the advantage of its vertical generalized coordinate system, thereby influencing the performance of its variables.

The CMEMS product used in this study is identified as GLOBAL_ANALYSIS_FORECAST_PHY_001_024. CMEMS analysis uses version 3.1 of nucleus for European modeling of the ocean (NEMO, Madec et al., 2008), based on the ORCA 1/12° grid (Madec & Imbard, 1996), with 50 levels for the vertical discretization, ranging

from 1 m resolution at the surface and to 450 m at the bottom, retaining 22 levels within the upper 100 m. The effects of tides and surface waves are excluded in this system. CMEMS database (including satellite altimeter data and SSTs; in situ temperature and salinity vertical profiles from CORIOLIS data, Cabanes et al., 2013; sea ice concentration from CERSAT, Girard-Ardhuin & Ezraty, 2012) are assimilated into the operational forecast model of the global ocean by means of a reduced-order Kalman filter with a 3-D multivariate modal decomposition of the forecast error and a 7-day assimilation cycle (Lellouche et al., 2013).

These two aforementioned global high-resolution ocean analyses, HYCOM and CMEMS, are used to conduct intercomparisons with FIO-COM analysis. These three global analyses are produced by three different ocean models, namely HYCOM, NEMO and modified MOM5, respectively. Only Argo temperature and salinity profiles were included in the FIO-COM assimilation, while there are more in situ observations assimilated into CMEMS and HYCOM analyses. Additional details regarding the distinguishing features for each analysis are given in Table 1.

2.3. Observations

In terms of observations, a gridded temperature and salinity data set, denoted as the Grid point value of the Monthly objective analysis, using the Argo data (MOAA GPV), is used to provide the monthly mean observations (Hosoda et al., 2008). The MOAA GPV data set is created using a 2-D optimal interpolation method with Argo data, TRITON mooring data and available CTD data to reconstruct the global temperature and salinity profiles. Because this data set is provided by the Japan agency for marine-earth science and technology (JAMSTEC), at http://www.jamstec.go.jp/ARGO/argo_web/argo/?page_id=83&lang=en, it is hereafter denoted as the JAMSTEC data set.

The World Ocean Atlas 2013 (WOA13) version 2 provides 1° gridded, objectively analyzed, climatological monthly fields of in situ temperatures (Locarnini et al., 2013). This data set is used to analyze and validate the SST variability for the aforementioned three analysis products, by comparisons with buoy SST observations during the 2015 *El Niño* year.

Multisourced in situ observations were also utilized, particularly datasets that have not been assimilated into the FIO-COM analysis. The Global tropical moored buoy array data set provides continuous buoy observations throughout the three tropical oceans, consisting of: (1) the Tropical atmosphere ocean (TAO)/Triangle trans-ocean buoy network (TRITON) array in the Tropical Pacific (Chiodi & Harrison, 2017; Kara et al., 2008b); (2) the Prediction and research moored array in the tropical Atlantic (PIRATA) (Da-Allada et al., 2017; Kara et al., 2008a); and (3) the Research moored array for African-Asian-Australian Monsoon Analysis and Prediction (RAMA) (Chen et al., 2017). The buoy locations are shown in Figure 1a.

Additional in situ observations are the EN4.2.1 data set (Good et al., 2013) from the UK Met Office (https://www.metoffice.gov.uk/hadobs/en4/). The EN4.2.1 data set provides abundant quality-controlled individual observations of ocean temperature and salinity profiles, which can further extend the validation of FIO-COM to subsurface layers. Due to the expensive calculations required to make the comparison, we only present comparisons for February and August of 2015, validating the general performance of FIO-COM in winter and summer. In total, there are 10,027 profiles in February 2015 (Figure 1b) and 12,423 profiles in August 2015 (Figure 1c) located in our area of focus (25°S-25°N, 180°W-180°E).

3. Seasonal Variability of MLD in the Tropical Oceans

3.1. MLD Definition

The criteria to define MLD in tropical oceans are not unequivocal, that is, based on fixed temperature differences, or fixed density differences, or a variable density criterion (de Boyer Montégut et al., 2004; Kara et al., 2000; Monterey & Levitus, 1997). Compared to other methods, temperature-based MLD estimates may be more reliable and simple in calculating the averaged MLD fields, with a specified temperature difference of 0.2°C or 0.5°C (Carton et al., 2008; Lee et al., 2015). de Boyer Montégut et al. (2004) report that

Journal of Geophysical Research: Oceans

10.1029/2020JC016118

Table 1
Parameters Comparison Among the Three Analyses Products

Analysis product	FIO-COM	CMEMS	HYCOM
Ocean model	Modified MOM5	NEMO v3.1	HYCOM
Surface wave model	MASNUM; nonbreaking surface wave-induced mixing (*Bv*)	-	-
Ice model	SIS	LIM2	-
Horizontal resolution	Global 1/10°	Global 1/12°	Global 1/12°
Vertical Layers	54 vertical layers with depth intervals varying smoothly from 2 m at the surface to 366 m at the bottom.	50-level vertical discretization of 1 m at surface decreasing to 450 m at bottom; retaining 22 levels within the upper 100 m.	40 standard z-levels
Temporal coverage	2014.01.01-present	2006.12.27-present	2012.05-present
Assimilated variables and observational data	MW_IR SST; Altimeter MSLA; Argo T&S profiles.	Altimeter along track SLA and MDT data; in situ T&S profiles from Coriolis GDAC; Reynolds AVHRR 0.25° SST; Sea-ice concentration and/or thickness from CERSAT.	SST (NOAA-18, NOAA-19, METOP-A, METOP-B, GOES-13, GOES-15, MSG, COMS-1, MTSAT-2, WindSAT, NPP-VIIRS, drifting buoys, fixed buoys, ships (ERI, bucket, hull contact)); SSH (Jason-2, Altika, Cryosat-2); In situ profiles (Argo, gliders, XBTs, fixed and drifting buoys, CTDs); sea ice concentration (SSM/I, SSMIS)
Assimilation scheme	EAKF data assimilation	"Mercator Assimilation System" version 2 (SAM-2), reduced-order Kalman filter based on the SEEK formulation with a 3DVAR bias correction for temperature and salinity	NCODA system
Outputs	T/S/U/V/SSH	T/bottomT/S/SSH/U/V/MLD/SIC/SIT/SIUV	T/S/U/V/SSH

Abbreviations: CMEMS, copernicus marine and environment monitoring service; FIO-COM, First Institute of Oceanography Coupled Ocean Model; HYCOM, hybrid isopycnal-sigma-pressure coordinate ocean model; JAMSTEC, Japan agency for marine-earth science and technology; MLD, mixed layer depth; MOM5; modular ocean model version 5, NEMO; nucleus for European modeling of the ocean, SIS, sea ice simulator; SSH, sea surface height; SST; sea surface temperature.

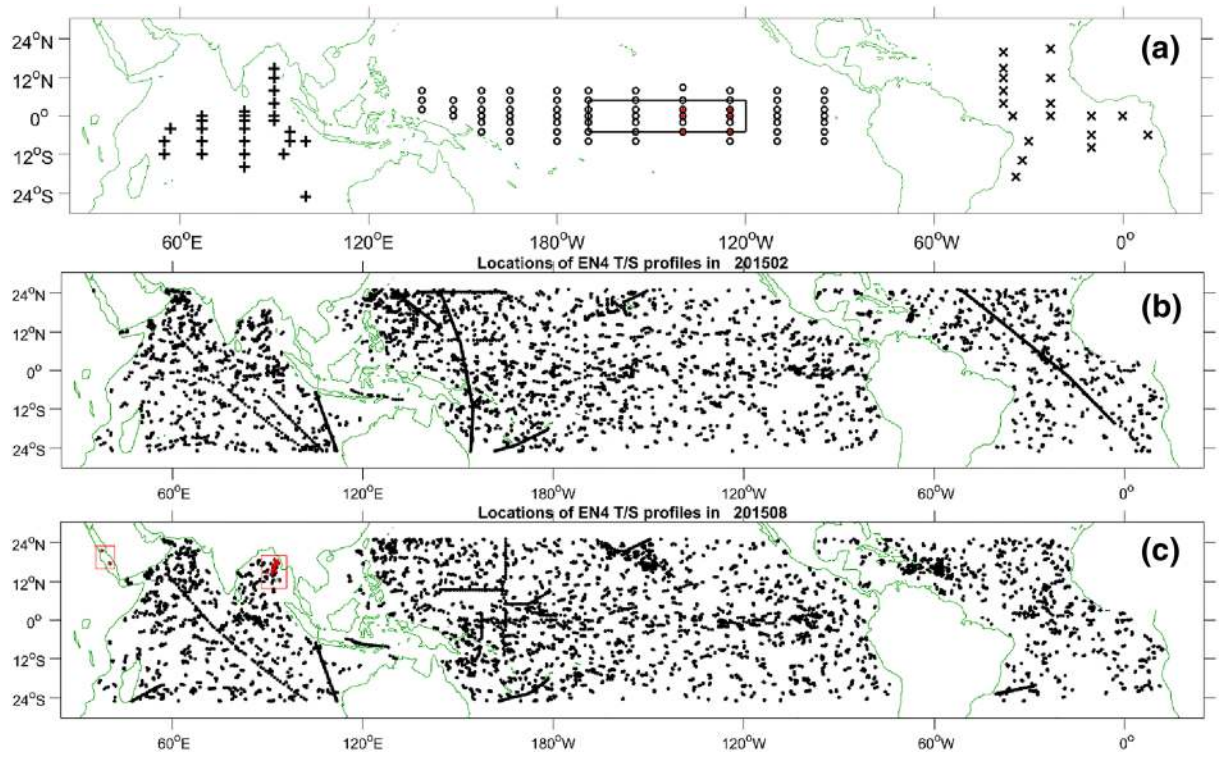

Figure 1. (a) Locations of TAO/TRITON (circles), PIRATA (crosses), and RAMA (pluses) moored buoys. The black box represents the region for the Niño 3.4 index; the red dots represent the buoys used in evaluating the SST variability during the 2015 *El Niño* event as discussed in Section 5. (b) Locations of EN4 profiles (dots) in February 2015. (c) Locations of EN4 profiles (dots) in August 2015, and red dots in red box is where FIO-COM has abnormal values. FIO-COM, First Institute of Oceanography Coupled Ocean Model; PIRATA, prediction and research moored array in the tropical Atlantic; RAMA, research moored array for African-Asian-Australian Monsoon analysis and prediction; SST, sea surface temperature; TAO/TRITON, tropical atmosphere ocean/triangle trans-ocean buoy network.

the MLD values estimated from the average-profile for climatology are globally 25% shallower than those estimated from individual profiles, with the same $\Delta T = 0.2°C$ criterion. This result suggests that artificially higher values of the ΔT criterion are usually needed in order to determine the MLD climatology. Monterey and Levitus (1997) used a criterion of $\Delta T = 0.5°C$ to estimate the climatological monthly mean MLD maps for the global ocean; Foltz et al. (2003) also used the $\Delta T = 0.5°C$ criterion to calculate MLDs in the tropical Atlantic Ocean.

In this paper, we adopt the temperature criterion $\Delta T = 0.5°C$, to calculate the MLD from the monthly average temperature profiles in the tropical oceans. The temperature difference is calculated relative to the temperature at the surface layer for each data set. We do not interpolate the analysis datasets vertically to the same vertical distribution as JAMSTEC, because one of our goals is to examine the accuracy of each analysis data set with respect to MLD estimates. The vertical interpolation will increase uncertainty in MLD estimates for each analysis, due to the relative coarse vertical resolutions of JAMSTEC (Figure 2). Additional problems related to the effect of salinity on the MLD and the barrier layer, are not considered in this study.

3.2. Intercomparison of Seasonal MLD From Analyses

The capability of FIO-COM to produce both the temporal variability and spatial structure of the MLD in tropical oceans is examined first. We process the aforementioned datasets of FIO-COM, HYCOM, CMEMS, and JAMSTEC to get the monthly mean temperature (T) profiles, then we calculate the MLD by setting the cutoff of the temperature difference at $\Delta T = 0.5°C$. MLD computed from the JAMSTEC data set can be considered as the observational reference or "*truth*".

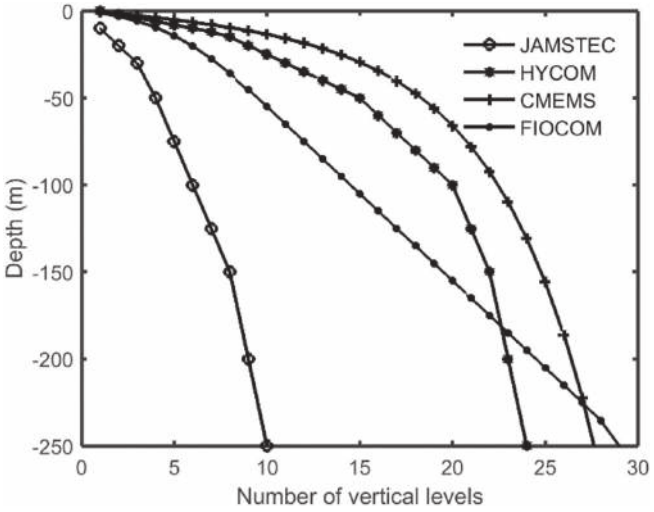

Figure 2. Vertical resolutions for each data set above 250 m depth.

Figure 3 shows comparisons of two-year seasonal averaged MLDs over the global tropical oceans for latitudes spanning from 25°S to 25°N, among JAMSTEC, FIO-COM, CMEMS and HYCOM datasets. Seasonal MLD variabilities in the tropical oceans are significant and, therefore can easily be observed in JAMSTEC data as well as the three analyses. The definitions of boreal winter, spring, summer and autumn in this paper are: December-January-February (DJF), March-April-May (MAM), June-July-August (JJA), and September-October-November (SON), respectively. Figure 4 shows the MLD differences from each analysis minus JAMSTEC observations, corresponding to the results shown in Figure 3. Table 2 presents the statistics, including Root mean square (RMS) errors and correlation coefficients (CR), of the seasonal MLD comparisons of the three analyses with respect to JAMSTEC. Here RMS and CR are computed using standard expressions as follows:

$$\mathrm{RMS} = \sqrt{\frac{1}{N}\sum_{i=1}^{N}\left(X_i - Y_i\right)^2} \tag{3}$$

$$\mathrm{CR} = \frac{1}{N-1}\sum_{i=1}^{N}\left(\frac{X_i - \frac{1}{N}\sum_{i=1}^{N}X_i}{STD(X)}\cdot\frac{Y_i - \frac{1}{N}\sum_{i=1}^{N}Y_i}{STD(Y)}\right) \tag{4}$$

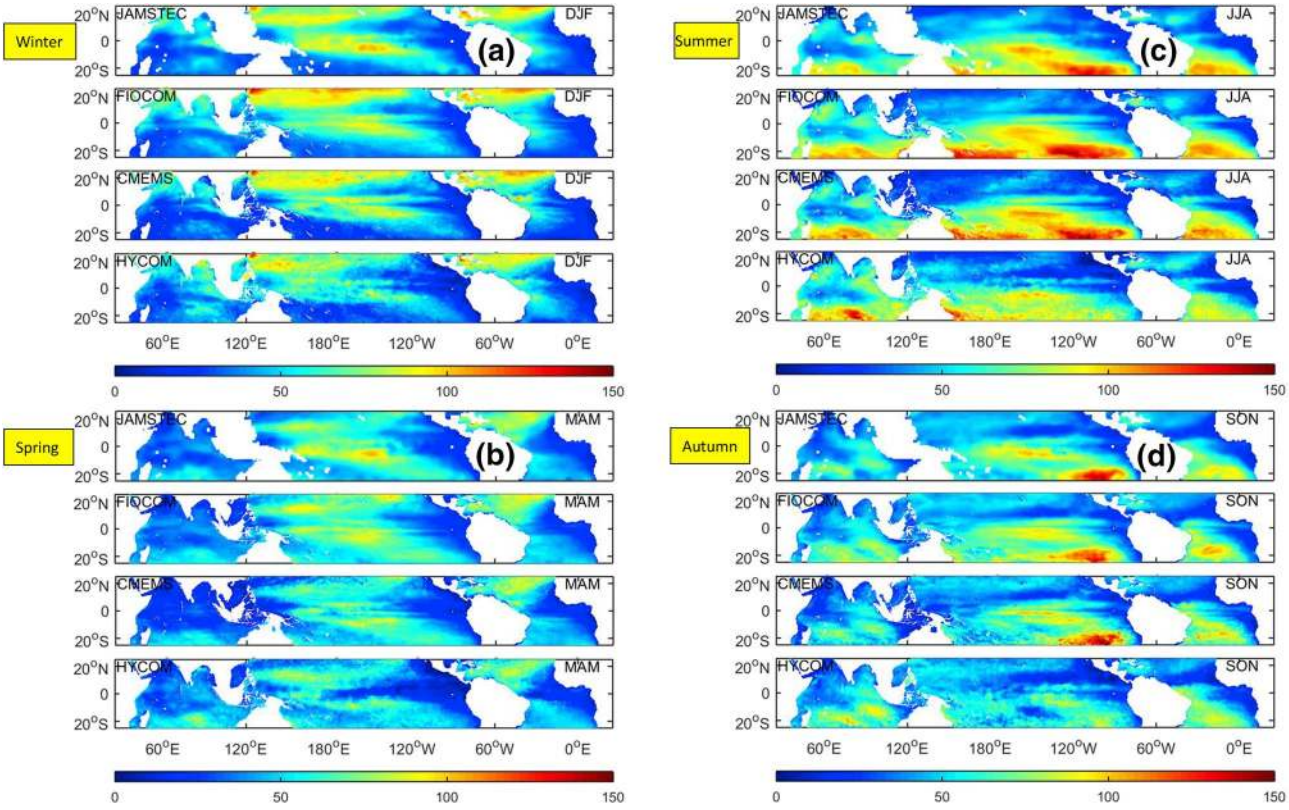

Figure 3. Two-year seasonal average MLD calculated from JAMSTEC, FIO-COM, CMEMS, and HYCOM datasets in the tropical oceans (25°S-25°N, 180°W-180°E) for: (a) DJF (Winter); (b) MAM (Spring); (c) JJA (Summer); and (d) SON (Autumn). All plotting is with respect to the same color bar range from 0 to 150 m. CMEMS, copernicus marine and environment monitoring service; DJF, December-January-February; FIO-COM, First Institute of Oceanography Coupled Ocean Model; HYCOM, hybrid isopycnal-sigma-pressure coordinate ocean model; JAMSTEC, Japan agency for marine-earth science and technology; JJA, June-July-August; MAM, March-April-May; MLD, mixed layer depth; SON, September-October-November.

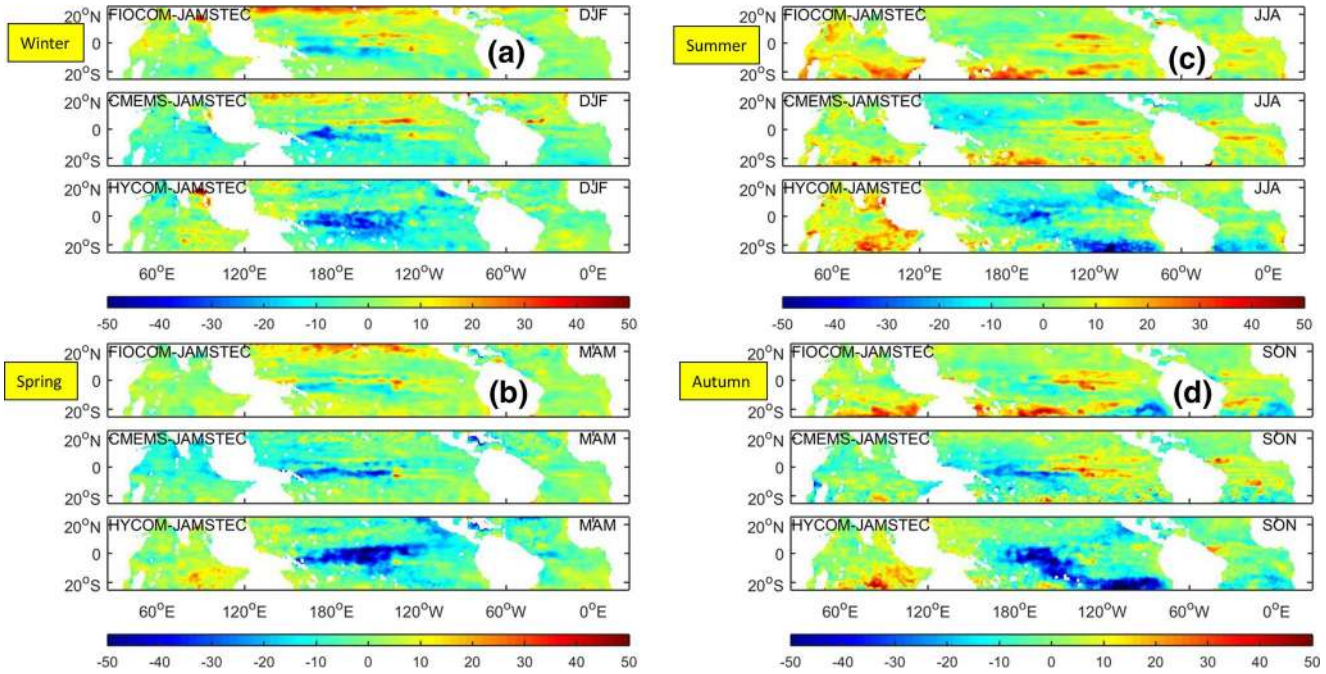

Figure 4. Difference of two-year seasonal average MLD between FIO-COM and JAMSTEC, CMEMS and JAMSTEC, HYCOM and JAMSTEC in (25°S-25°N, 180°W-180°E) for: (a) DJF (Winter); (b) MAM (Spring); (c) JJA (Summer); and (d) SON (Autumn). All plotting are in the same color range from −50 to 50 m. CMEMS, copernicus marine and environment monitoring service; DJF, December-January-February; FIO-COM, First Institute of Oceanography Coupled Ocean Model; HYCOM, hybrid isopycnal-sigma-pressure coordinate ocean model; JAMSTEC, Japan agency for marine-earth science and technology; JJA, June-July-August; MAM, March-April-May; MLD, mixed layer depth; SON, September-October-November.

where N is the total number of points; X represents the analyses data, Y represents the observations and each pair is denoted by (X_i, Y_i); STD (X) and STD (Y) denote the calculated standard deviations.

Figure 3a displays the MLDs in the boreal winter (DJF). Relatively deep MLDs are observed to be distributed mostly in the northern and central parts of the tropical Pacific, and the northern part of the tropical Atlantic in the JAMSTEC observations. The MLD differences, as shown in Figure 4a, reveal more quantitative bias features in each analysis. FIO-COM has a positive bias area in the northern part of the tropical Pacific over latitudes that span from 20°N to 25°N and a small negative bias area in the central tropical Pacific. For CMEMS, the spatial distribution of biases is similar to those of FIO-COM, that is, a positive bias area in the northern part of tropical Pacific but not as large as that in FIO-COM. CMEMS's negative biases appear in the central tropical Pacific Ocean but are distributed over a much broader area than those from FIO-COM. For HYCOM, the negative bias areas are quite obvious in most of the tropical Pacific Ocean. FIO-COM, CMEMS, and HYCOM can all produce reasonable simulations of MLD in most areas of both the tropical Indian and Atlantic Oceans, except for a relatively small area in the Bay of Bengal, where the differences of both FIO-COM and HYCOM, with respect to JAMSTEC, are positive and substantial; this result could be due to the difficulty in simulating the very low sea surface salinity in this area (Grunseich et al., 2011; Li et al., 2016; Subrahmanyam et al., 2011; Thompson et al., 2006). CMEMS exhibits a small area of negative biases with respect to JAMSTEC along the equatorial Indian Ocean.

Table 2
Statistics of Seasonal MLD for FIO-COM, CMEMS, and HYCOM With Respect to JAMSTEC Data

	FIO-COM		CMEMS		HYCOM	
Time	RMS(m)	CR (%)	RMS(m)	CR (%)	RMS(m)	CR (%)
DJF	8.6	93.0	9.4	92.4	11.2	88.5
MAM	7.8	92.0	9.3	89.5	13.1	76.2
JJA	10.1	95.5	9.5	95.2	12.7	87.6
SON	10.2	89.3	9.7	89.7	14.6	75

Abbreviations: CMEMS, copernicus marine and environment monitoring service; CR, correlation coefficient; FIO-COM, First Institute of Oceanography Coupled Ocean Model; HYCOM, hybrid isopycnal-sigma-pressure coordinate ocean model; RMS, root-mean-square error.

In the boreal spring (MAM), the MLD values experience shoaling over most of the tropical oceans as a result of weak Tropical Easterlies in both hemispheres (Figure 3b). Relatively deep MLDs are concentrated in the

central Pacific Ocean along the equator. As shown in Figure 4b, the differences of FIO-COM minus JAMSTEC are very small except for a positive difference area in the northern portion of the domain, indicating that FIO-COM produces high-quality simulations in most areas of the tropical oceans. CMEMS generally has small differences except for an obvious belt with negative biases in the central tropical Pacific, whereas HYCOM seems to notably underestimate the MLDs in the central tropical Pacific, with a relatively large area of significantly negative bias.

Seasonal variability in MLDs, changing from the boreal spring to the summer (JJA), is significant, especially in the southern part of the tropical oceans. In this transition season, MLDs become much deeper, with values exceeding 100 m in most of the tropical oceans in areas south of the equator, and up to 150 m in the southern part of the tropical Pacific (Figure 3c). Deeper MLDs indicate stronger mixing in these areas in the boreal summertime. The MLD spatial patterns obtained from FIO-COM analysis and CMEMS analysis agree relatively well with the observations (JAMSTEC), while the HYCOM analysis fails to reproduce these deep MLD features in the southern part of the tropical Pacific and Atlantic, to the extent that is shown in the observations. All the simulations seem to overestimate the MLDs in the Indian Ocean (Figure 4c). In the Pacific Ocean, the differences between both FIO-COM and CMEMS minus JAMSTEC are small over much of the tropical Pacific, but exhibit several belts of large positive biases distributed over the central and southern parts of this region. Like the results for summertime, HYCOM again underestimates the MLDs and gives results that have negative differences distributed over most of the tropical Pacific, as well as the southern part of the tropical Atlantic.

Although strong mixing also exists in the autumn (SON), with MLDs of up to 150 m, the spatial scales for these results are smaller than those in the summertime and concentrate in the southeastern part of the tropical Pacific (Figure 3d). Both FIO-COM and CMEMS reproduce the deeper MLDs in the same area quite well, while HYCOM fails to capture this evident autumn feature of the MLDs. Comparing the MLD differences of each simulation with observations (Figure 4d), we noticed that FIO-COM has stronger mixing than observations in the southern part of tropical Indian and Pacific Oceans, and weaker mixing in the southeastern portions of the tropical Pacific and tropical Atlantic. Compared to observations, CMEMS produces slightly shallower MLDs in the western part of the overall tropical domain but slightly deeper MLDs in the eastern portion of the tropical Pacific. Similar to the previous comparisons, HYCOM continues to underestimate the MLD in the Pacific and exhibits some overestimations in the southern part of the tropical Indian Ocean.

The overall-averaged RMS errors of MLD estimates from FIO-COM, CMEMS, and HYCOM, in comparison with JAMSTEC (Table 2), are 9.2, 9.5, and 12.9 m, respectively, and the corresponding correlation coefficients are 92.5%, 91.7%, and 81.8%. As shown in Table 1, there are many more in situ observational data assimilated into both CMEMS and HYCOM analyses, than into the FIO-COM analysis. Therefore, we are surprised to conclude that the FIO-COM analysis provides a comparable performance, in terms of the estimation of MLDs, indicating its advantage in subsurface simulations.

3.3. Seasonal Variations of MLD in Tropical Oceans

In the previous subsection, seasonal MLDs computed from all four datasets are displayed and the capability of the FIO-COM analysis is assessed through comparisons with JAMSTEC observations. An obvious question is this: To what extent might the seasonal MLD variations in the tropical oceans possibly change? While MLDs in most of the tropical oceans are less than 50 m (Figure 3), the amplitudes of seasonal variations could be relatively small. Therefore, we use a "ratio" instead of an "amplitude" to demonstrate the seasonal cycle of MLD,

$$Ratio = \left(MLD_{SSN} - MLD_{ANN}\right) / MLD_{ANN} \tag{5}$$

Ratios of seasonal MLD variations for the four seasons, as inferred from both JAMSTEC (observations) and FIO-COM (analysis), are presented in Figure 5. The objective of this section is: (1) to depict the seasonal variations of MLDs for years 2014 and 2015 in tropical oceans; and (2) to further validate the

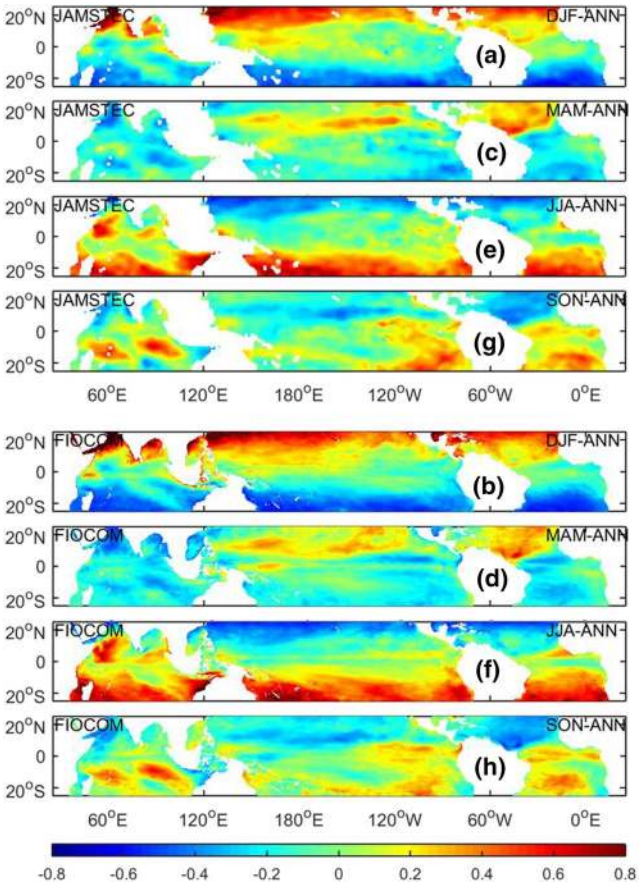

Figure 5. Ratios of MLD seasonal variations inferred from both JAMSTEC and FIO-COM for (a and b) Winter (DJF); (c and d) Spring (MAM); (e and f) Summer (JJA); and (g and h) Autumn (SON). Seasonal variations are calculated as the MLDs for each season minus the annual (ANN) mean MLDs; and the ratio is calculated by the seasonal variations of MLD compared to the annual mean MLD. DJF, December-January-February; FIO-COM, First Institute of Oceanography Coupled Ocean Model; JAMSTEC, Japan agency for marine-earth science and technology; JJA, June-July-August; MAM, March-April-May; MLD, mixed layer depth; SON, September-October-November.

FIO-COM analysis. Thus, through comparisons of MLD variation ratios for each season, we show that there is good overall agreement of seasonal MLD variations between FIO-COM analysis and JAMSTEC observations.

Generally, significant changes appear in both the boreal winter (DJF) and summer (JJA), with values for the ratio exceeding ±80% in the southern and northern tropical oceans. During the boreal winter (Figures 5a and 5b), MLDs strongly shoal in the southern tropical oceans (south of 10°S) due to weak winds and downward surface heat fluxes (Keerthi et al., 2013), but strongly deepen in the northern tropical oceans. Conversely, MLDs strongly deepen in the southern tropical oceans but shoal in the northern tropical oceans during the boreal summer (Figures 5e and 5f). MLD variations are relatively minor over the equatorial tropical oceans in both boreal winter and summer. The variation in the equatorial oceans (10°S-10°N) is generally within the range of 10%–20%, except in the northwestern Indian ocean, where there is a strong MLD deepening in the boreal summer at the southern Arabian Sea (Figures 5e and 5f). Anomalously strong monsoons are defined as years when the normalized Indian Monsoon Index is larger than 0.5 (Keerthi et al., 2013). The study by Wang et al. (2001) displays the Indian Summer Monsoon Index data from 1948 to 2015, showing larger indexes for the years 2014 and 2015 with values of −2.35 and −2.79 respectively (http://apdrc.soest.hawaii.edu/projects/monsoon/seasonal-monidx.html). Thus, summer monsoon winds in both 2014 and 2015 were stronger than usual, accounting for deeper MLDs in the southern Arabian Sea in Figures 5e and 5f.

In the boreal spring (Figures 5c and 5d), there is a modest MLD deepening belt around 10°-20°N latitudes along the intertropical convergence zone (ITCZ, 2°-8°N) over the northern tropical Pacific Ocean. Moreover, MLD shoaling areas are observed in the east-central equatorial Pacific, which should be caused by the strong 2015 *El Niño* event (see Section 5). Moderate MLD shoaling is observed in most of the tropical Indian Ocean and western tropical Pacific. Relatively strong MLD deepening occurs in the tropical North Atlantic as a result of the negative Atlantic meridional mode (AMM) event in 2015, with cold SST anomalies in the tropical North Atlantic during March-May and comparably warmer SST anomalies in the tropical South Atlantic (see Figure 2 in Rugg et al., 2016).

MLD variations in boreal autumn (Figures 5g and 5h) are almost the reverse to the features occurring in spring. Except for the Arabian Sea, MLD shoaling is as strong as in spring. In the southern Indian Ocean, two positive areas of MLD variations appear in contrast to the negative values in spring, but with larger magnitude. Recent research from Australian bureau of meteorology suggests that a positive Indian Ocean dipole (IOD) peaked in the autumn of 2015 in the tropical Indian Ocean (http://www.bom.gov.au/climate/iod/). A positive IOD event over the Indian Ocean is equivalent to *El Niño*, with warm SST anomalies occurring in the eastern basin of the Indian Ocean and cold SST anomalies in the waters off Sumatra (Keerthi et al., 2013; Saji et al., 1999), strengthening the MLD deepening in the southern Indian Ocean in autumn.

Compared to the JAMSTEC results, the FIO-COM analysis generally perfo rms well in terms of reductions to the MLD seasonal variations over the tropical oceans. Moreover, FIO-COM also captures these variations during the negative AMM (in spring) and positive IOD events (in autumn), but tends to overestimate the MLD deepening in the northwestern tropical Atlantic Ocean in the boreal winter.

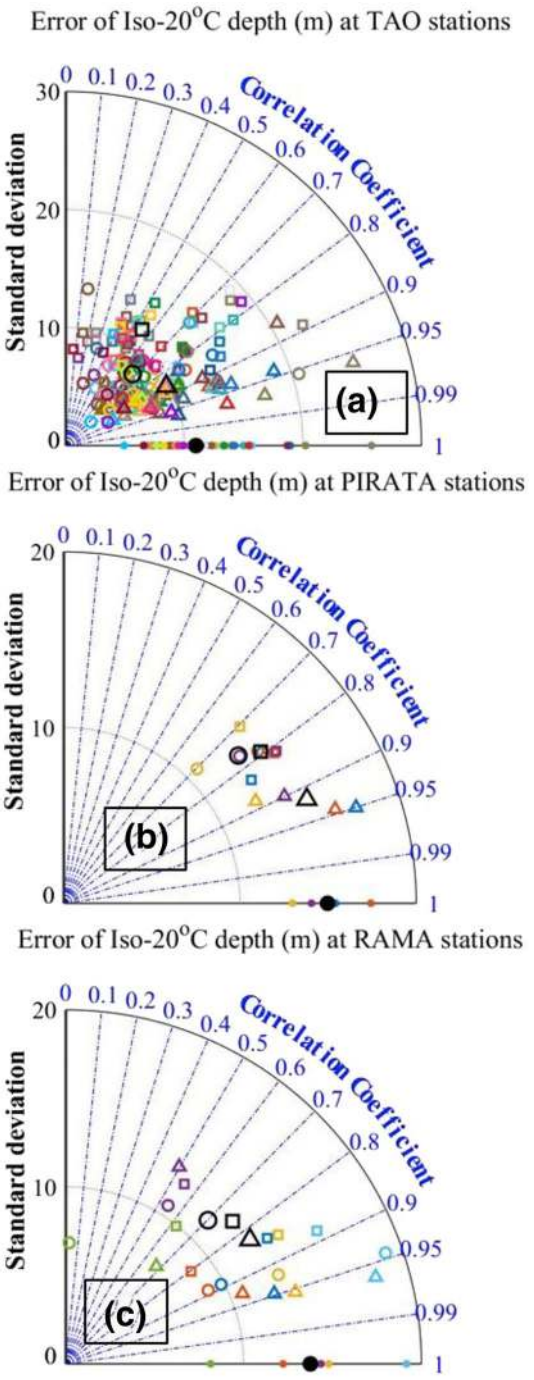

Figure 6. Taylor diagrams showing the quantitative assessment of FIO-COM, CMEMS, and HYCOM comparing to buoy observations from (a) TAO, (b) PIRATA, and (c) RAMA for the 20°C isothermal depth: The dots represent the buoy observations; circles represent FIO-COM; triangles represent CMEMS; and squares represent HYCOM. Black color represents the average error of all buoys; other colors represent the errors for different buoys. CMEMS, copernicus marine and environment monitoring service; FIO-COM, First Institute of Oceanography Coupled Ocean Model; HYCOM, hybrid isopycnal-sigma-pressure coordinate ocean model; PIRATA, prediction and research moored array in the tropical Atlantic; RAMA, research moored array for African-Asian-Australian Monsoon analysis and prediction; TAO, tropical atmosphere ocean.

4. Validation With Buoy and In Situ Observations

4.1. Comparisons With TAO, RAMA, and PIRATA in Tropical Oceans

Further validations using the 20°C isothermal depth and temperature at 5 m depth, are conducted using Taylor diagrams (Taylor, 2001), comparing each analysis (FIO-COM, CMEMS, and HYCOM) to all available observations at TAO, PIRATA, and RAMA buoys in years 2014 and 2015 (Figures 6 and 7). The standard deviation of each data set is displayed as the radial distance from the origin, the CR between the analyses and observations is the angle from the X-axis, and the RMS error is taken as the distance between the observations on the X-axis and the corresponding location of each analysis.

For the 20°C isothermal depth, there are more available buoy observations in the tropical Pacific Ocean region (Figure 6a) than in both the tropical Atlantic (Figure 6b) and Indian Oceans (Figure 6c). At TAO buoys, both FIO-COM and CMEMS analysis have high correlation coefficients with respect to the observations, while HYCOM has a relative low CR of 50% and large errors. HYCOM gives a relatively poor simulation of the temperature profiles in the tropical Pacific, which also is revealed in the validation of the MLDs (Section 3.2). In the tropical Atlantic Ocean, HYCOM and FIO-COM analyses have comparable performance results, with respect to PIRATA buoys, whereas CMEMS analysis achieves the best simulations, with a high CR of over 90%. In the tropical Indian Ocean (Figure 6c), all the three analyses perform well, with similar comparison results with respect to RAMA buoy observations.

SST is defined as the water temperature between 1 mm and 20 m below the ocean surface. Therefore, the temperature at 5 m depth is within this measurement interval for SST. SST is an assimilated variable in all the three analyses products; therefore, it is not surprising to find that the three analyses achieve better performance for temperature at 5 m depth (Figure 7), than for the 20°C isothermal depth (Figure 6). At TAO buoys, all the analyses show high correlation coefficients with values over 92%, and small RMS errors less than 0.57°C. Good performance results for all three analyses are observed at PIRATA buoys, with high correlation and small RMS errors. In the tropical Indian Ocean, both CMEMS and FIO-COM analysis have higher correlation coefficients (smaller RMS errors) than HYCOM, given as 94% (0.24°C), 88% (0.36°C), and 77% (0.50°C) respectively.

Generally, comparing the validation statistics of these three simulations, we can conclude that CMEMS achieves the best simulation, and FIO-COM is better than HYCOM. However, as mentioned previously, the observations from the Global tropical moored buoy array (TAO, PIRATA, and RAMA), used for model assessment here, have been assimilated into CMEMS and HYCOM analyses, whereas FIO-COM does not assimilate these data.

4.2. Comparisons With EN4 Temperature and Salinity Profiles

The EN4 data set provides quality-controlled individual profiles of temperature and salinity observations. Figures 1b and 1c shows the locations of all the available EN4 profiles in February and August of 2015 respec-

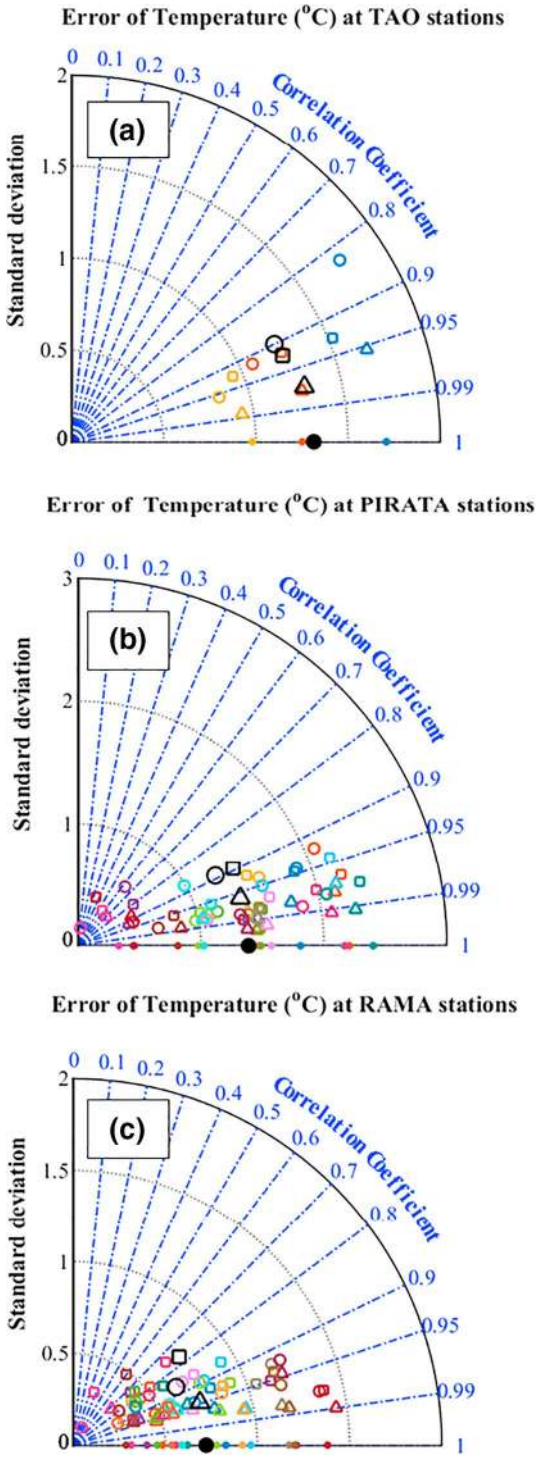

Figure 7. Taylor diagrams showing the quantitative assessment of FIO-COM, CMEMS, and HYCOM comparing to buoy observations from (a) TAO, (b) PIRATA, and (c) RAMA for the Temperature at 5 m depth: The dots represent the buoy observations; circles represent FIO-COM; triangles represent CMEMS; and squares represent HYCOM. Black color represents the average error of all buoys; other colors represent the errors for different buoys. CMEMS, copernicus marine and environment monitoring service; FIO-COM, First Institute of Oceanography Coupled Ocean Model; HYCOM, hybrid isopycnal-sigma-pressure coordinate ocean model; PIRATA, prediction and research moored array in the tropical Atlantic; RAMA, research moored array for African-Asian-Australian Monsoon analysis and prediction; TAO, tropical atmosphere ocean.

tively, which are applied to validate the daily values of the analysis datasets. This comparison consists of three steps. First, the three analyses are interpolated spatially to the locations of individual EN4 observations. Second, temporal interpolation is conducted to match the times of the analyses data to the observational times. Third, as the observational depths are not uniform for the EN4 profiles, therefore, vertical interpolation is also conducted.

Figures 8 and 9 show the scatter comparisons of temperature and salinity in August of 2015 at depths of 10, 100, 300, and 600 m. The statistical results for mean error (ME), RMS error, and CR also show the quantitative performance of the analyses. For salinity (Figure 8), all the three analyses show a good agreement with EN4 observations, with smaller RMS errors and MEs, and higher CR values, as depths increase. At 10 m depth, where more observations (7,300 points in total) are available, the CMEMS analysis gives the best performance with an RMS error of 0.2 PSU and CR of 98%; FIO-COM analysis shows a larger RMS error (0.4 PSU) and a lower correlation (92%). The overestimates in the FIO-COM analysis are mainly attributed to locations where observed salinity is over 38 PSU or less than 32 PSU. Locations with observed salinity over 38 PSU occur in the Red Sea (in the left box in Figure 1c), one of the most salty bodies of water in the world, with an average of 40 PSU. These particular high salinity scatters exist at levels of 10, 100, and 300 m. At these points, HYCOM and CMEMS analyses agree well with the EN4 observations, very close to the regression lines. However, it is important to note that the assimilated observations in the three analysis datasets share some data with the EN4 data set. Both Argo data and other in situ profiles have been assimilated into CMEMS and HYCOM analyses (https://www.godae-oceanview.org/science/ocean-forecasting-systems/assimilation-characteristics/), while only Argo data is assimilated into FIO-COM analysis. Therefore, it is not surprising that CMEMS and HYCOM analyses have better performances. The in situ profiles in the Red Sea are excluded in the FIO-COM analysis, accounting for its overestimation for salinity at these points by 2.8 PSU (at 10 m depth), 1.4 PSU (at 100 m), and 0.4 PSU (at 300 m). The points with observed salinity less than 32 PSU are concentrated in the Bay of Bengal (in the box on the right in Figure 1c), where the salinity of the upper layer is remarkably low owing to the huge freshwater input from the Ganges-Brahmaputra-Meghna river system. In Figure 8 at the 10 m depth comparison, both FIO-COM and HYCOM analyses overestimate the salinity at these points, by 1.3 and 1.5 PSU respectively, whereas the CMEMS analysis shows better agreement by 0.2 PSU deviation.

All three analyses perform well in temperature (Figure 9), with respect to EN4 observations. For each analysis, the change in RMS errors, with increasing depth, shows a similar trend, with among the smallest values at the surface layer (10 m), increasing to the largest errors around 100 m depth, then decreasing with increasing depths, again. As mentioned above, in situ T/S profiles and Argo data have been assimilated into HYCOM and CMEMS analyses; and the best agreement is achieved by CMEMS. However, the FIO-COM analysis has smaller RMS errors and higher correlation coefficients than those of the HYCOM analysis at the 100 m depth, despite not assimilating in situ observed temperature profiles. This strong performance of FIO-COM analysis in simulating the mixed layer, can be attributed to the addition of the nonbreaking wave term. But this hypothesis needs to be confirmed with further sensitivity experiments.

We also present the zonal RMS profiles of temperature and salinity in both February and August in Figures 10 and 11 respectively, giving comprehensive pictures of the performance of the three analyses in producing temperature and salinity profiles (from the surface to 1,000 m depth). Zonal averaged RMS profiles are calculated using all available data in consecutive latitude spans of 0.5° increments, from the surface to the 1,000 m depth. Generally, all three analyses datasets provide reliable simulations of temperature and salinity profiles, with RMS errors for salinity and temperature in the range of about 0–0.5 PSU and 0 ~ 2°C, respectively. For the salinity profiles (Figures 10a–10c and 11a–11c), large RMS errors from FIO-COM analysis mostly occur in the upper 100 m layers from 20°S to 25°N. HYCOM analysis has large RMS in the upper 200 m layers from 15°S to 20°N. CMEMS analysis gives the best performance with small RME errors and the relatively large errors, mostly occurring in the shallow surface layer. For the temperature profiles (Figures 10d–10f and 11d–11f), high accuracy of SSTs is attributed to the assimilation of SST observations into all three analyses. However, all three analyses have the same common problem of large temperature RMS in the subsurface mixing layer, due to different mixing parameterizations applied in the respective ocean models. Although the in situ T/S profiles included in EN4 have been assimilated into both HYCOM and CMEMS analyses, while not in FIO-COM analysis, FIO-COM is still able to

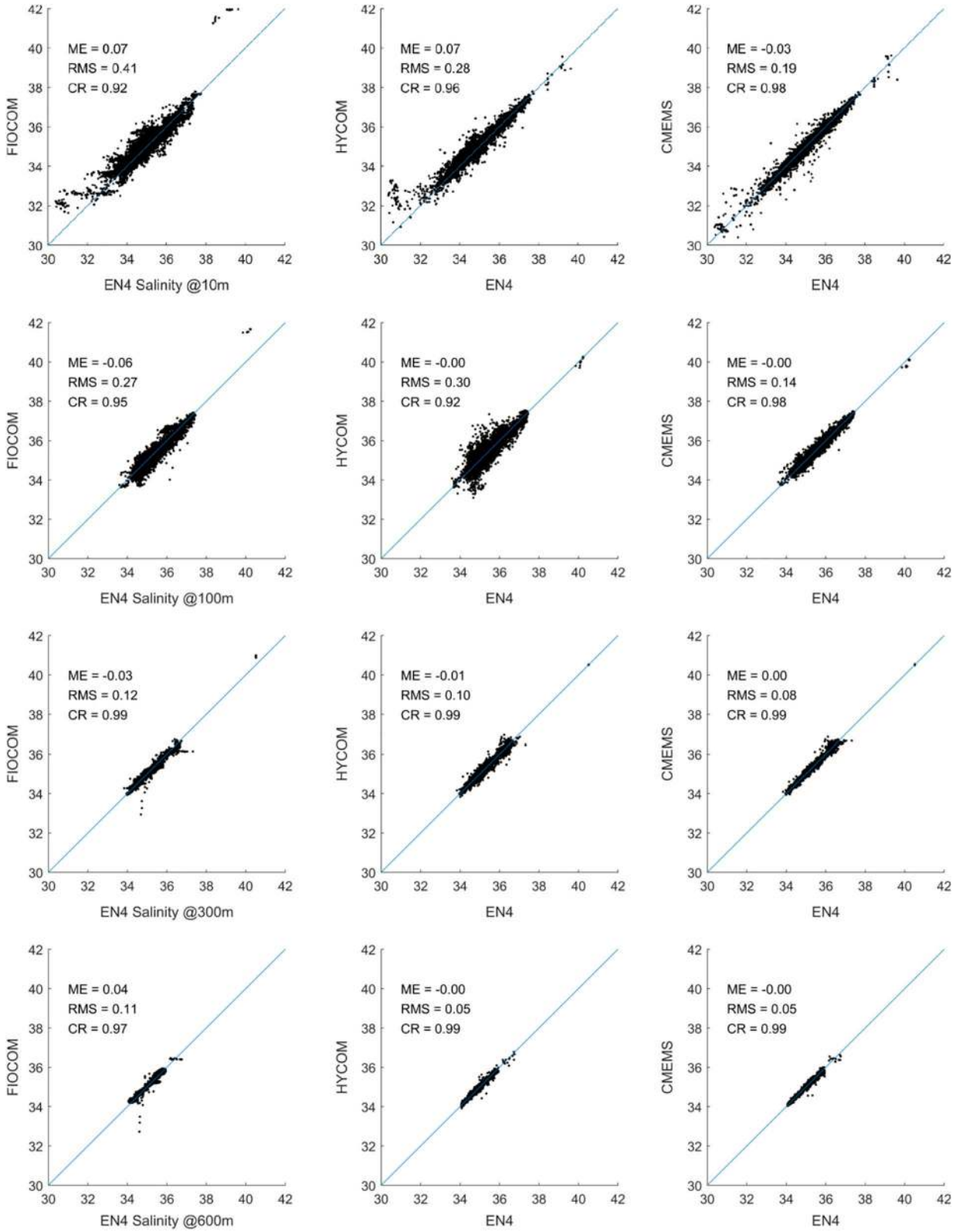

Figure 8. Scatterplots of salinity between EN4 observations and FIO-COM, HYCOM, CMEMS analyses in August 2015, at depths of 10, 100, 300, and 600 m, respectively. FIO-COM, First Institute of Oceanography Coupled Ocean Model; CMEMS, copernicus marine and environment monitoring service; HYCOM, hybrid isopycnal-sigma-pressure coordinate ocean model.

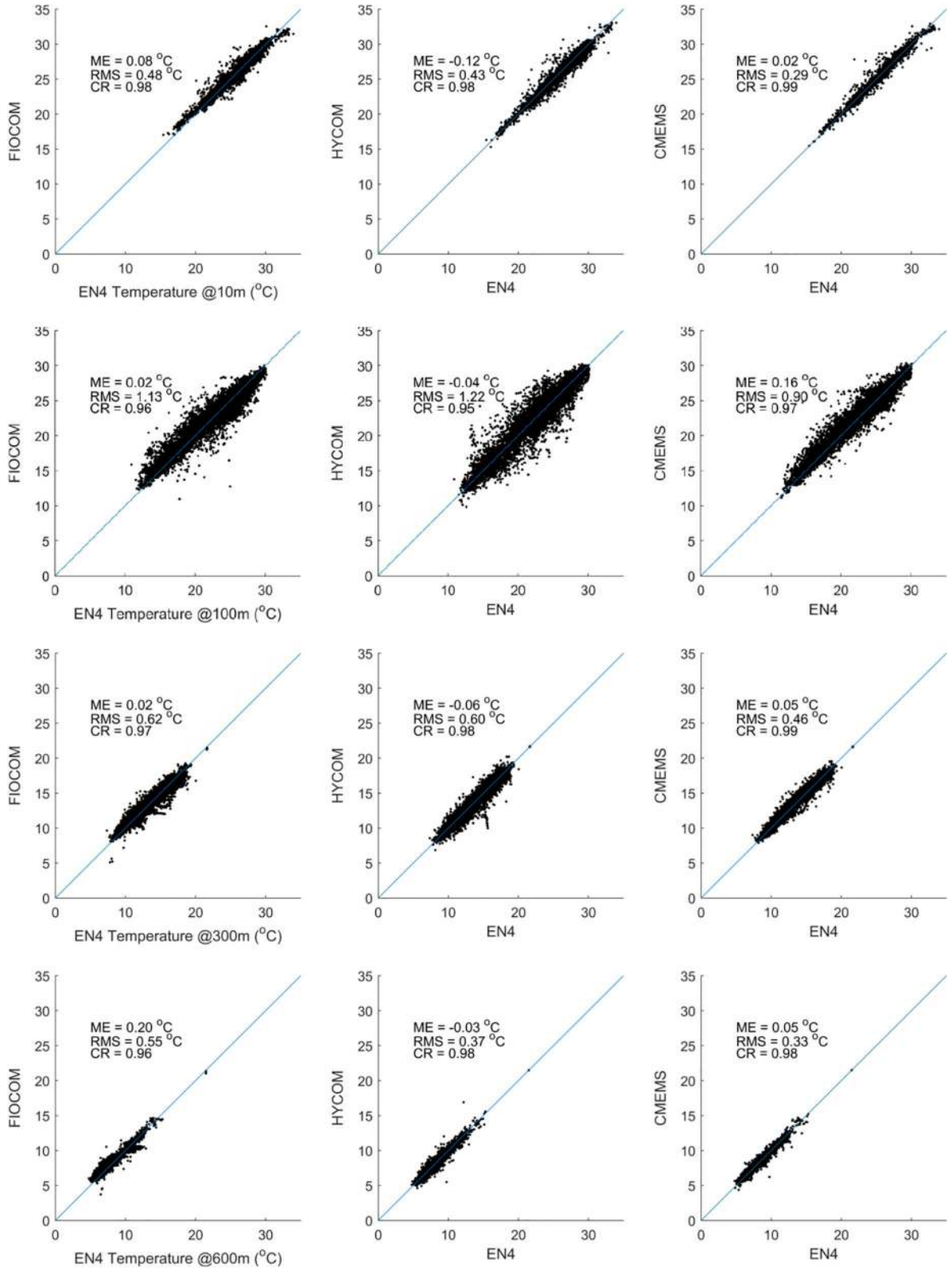

Figure 9. Scatterplots of temperature between EN4 observations and FIO-COM, HYCOM, CMEMS analyses in August 2015, at depths of 10, 100, 300, and 600 m, respectively. CMEMS, copernicus marine and environment monitoring service; FIO-COM, First Institute of Oceanography Coupled Ocean Model; HYCOM, hybrid isopycnal-sigma-pressure coordinate ocean model.

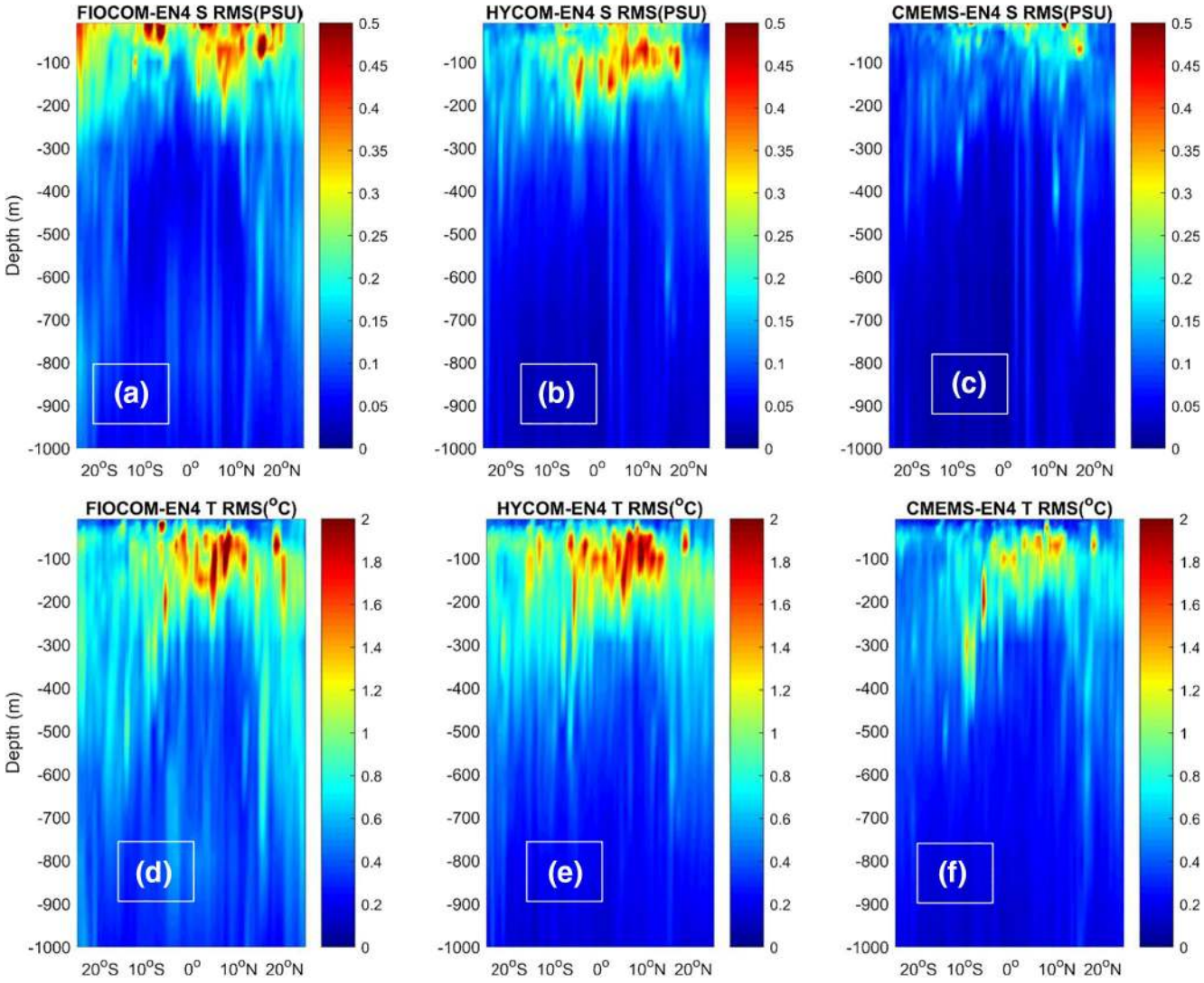

Figure 10. Zonal RMS error profiles of Salinity (upper panel) and Temperature (lower panel) for FIOCOM (a and d), HYCOM (b and e), and CMEMS (c and f) with respect to EN4 individual observations in February 2015. CMEMS, copernicus marine and environment monitoring service; FIO-COM, First Institute of Oceanography Coupled Ocean Model; HYCOM, hybrid isopycnal-sigma-pressure coordinate ocean model; RMS, root mean square.

provide good results for temperature profiles, especially in the southern portions of the tropical oceans (Figure 11d).

We display the averaged RMS of temperature and salinity for the entire study region (25°S-25°N, 180°W-180°E) in February 2015 (Figure 12a) and August 2015 (Figure 12b). For salinity, RMS errors are large near the ocean surface, and decrease with increasing depth. The values for salinity RMS are small; FIO-COM analysis has the largest RMS in the surface layer, up to 0.4 PSU. For temperature, RMS errors increase from small values near the surface, reaching a peak at depths of about ~100 m, then decrease with the increasingly deep ocean. CMEMS has the best performance, which may be attributed to the state-of-the-art ocean model and abundant data set of assimilated in situ temperature and salinity observations, assimilated into the analysis. These data are also assimilated into the HYCOM analysis. However, it is surprising to observe that the FIO-COM analysis has a better performance than HYCOM in the layers between 50 m and 150 m; whereas the in situ temperature and salinity profiles have not been assimilated into FIO-COM.

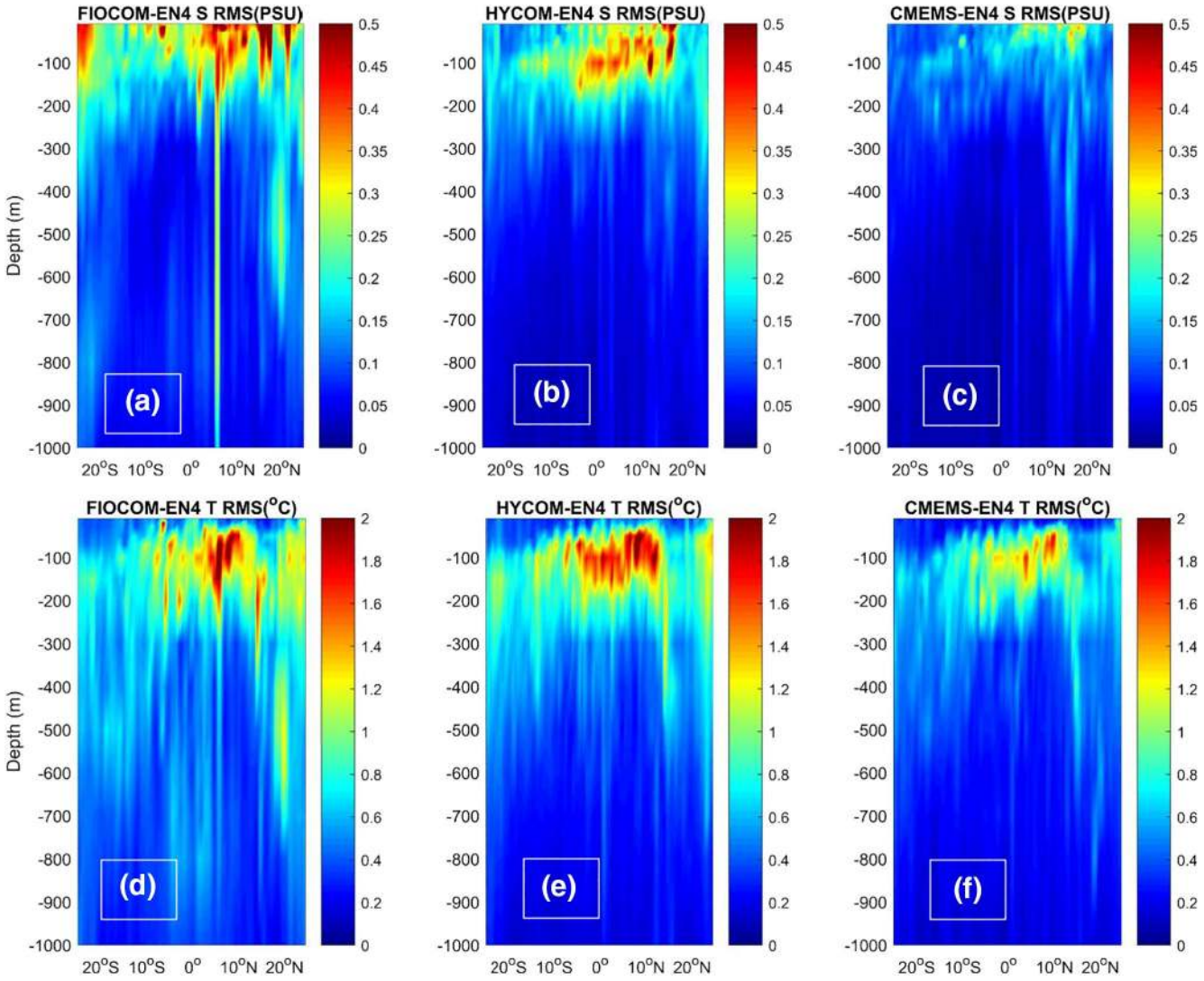

Figure 11. Zonal RMS error profiles of Salinity (upper panel) and Temperature (lower panel) for FIOCOM (a and d), HYCOM (b and e), and CMEMS (c and f) with respect to EN4 individual observations in August 2015. CMEMS, copernicus marine and environment monitoring service; FIO-COM, First Institute of Oceanography Coupled Ocean Model; HYCOM, hybrid isopycnal-sigma-pressure coordinate ocean model; RMS, root mean square.

5. SST Variability During 2015 *El Niño* Event

In this section, we continue to investigate the performance of FIO-COM analysis in simulating the daily SSTs during the 2015 *El Niño*, which began as a weak *El Niño* in April 2015 and developed into a strong *El Niño* during the winter of 2015/2016.

Instead of calculating the sea surface temperature anomaly (SSTA) in the *Niño* 3.4 region (bounded by the region 5°S-5°N and 170°W-120°W), we investigate the SST variability, instead of SSTA variability. This is done by comparing CMEMS, FIO-COM and HYCOM analysis, with the objectively analyzed climatological monthly mean SSTs from WOA13, and with the SST observations from the TAO buoys located in the *Niño* 3.4 region (shown in Figure 1a). The observations at buoy (5°N, 140°W) in 2015 are not included because of quality issues; therefore, 19 buoys in total are applied in the validation here.

The statistics in Table 3 are also presented in a bar plot (Figure 13). Overall, CMEMS analysis achieves the lowest values for the RMS errors and highest correlation coefficients at most of the buoys, except for the buoy at 5°S and 125°W, where the RMS error of CMEMS is 0.44°C, higher than values of either FIO-

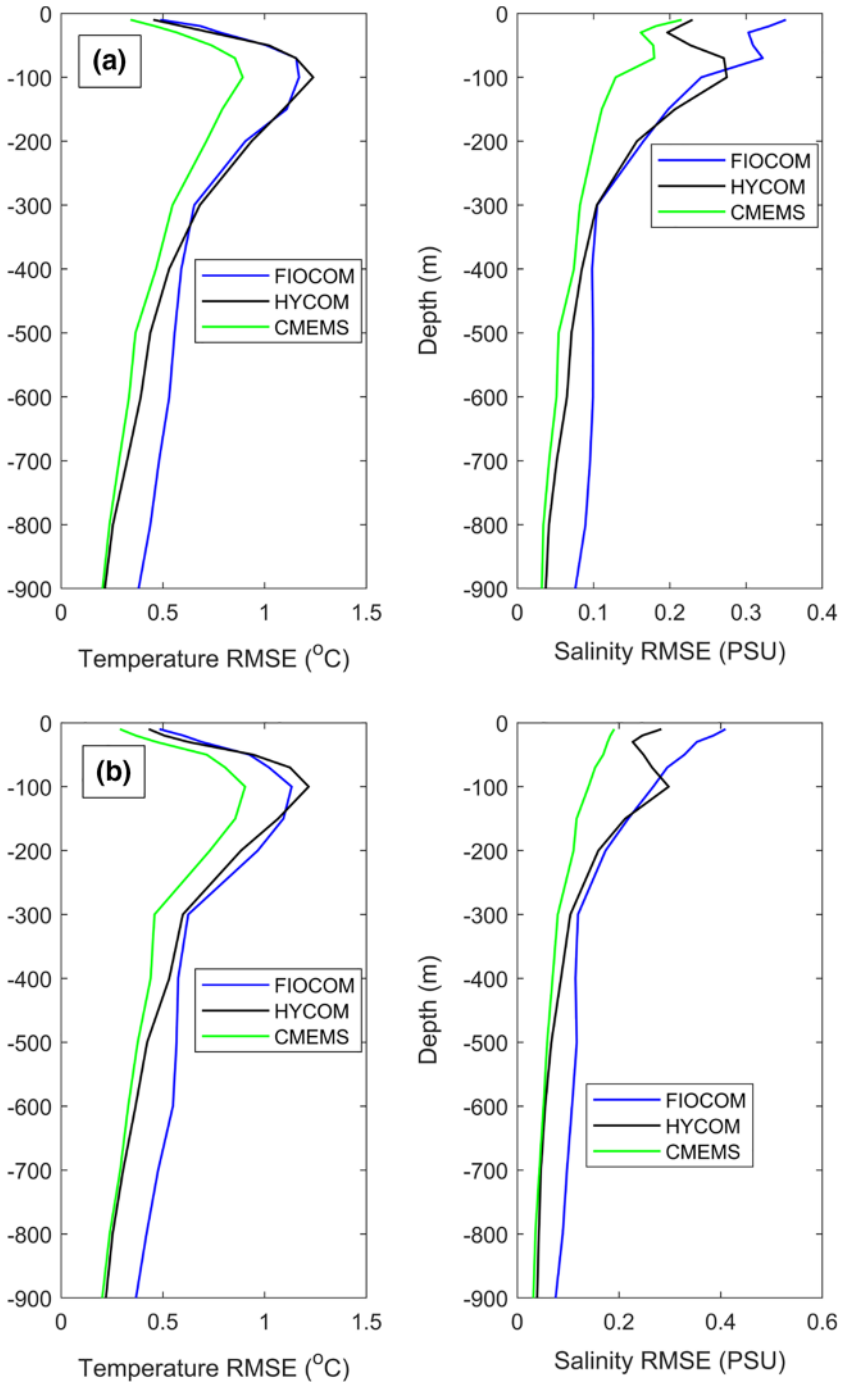

Figure 12. Average RMS errors of temperature and salinity for the three analyses compared to EN4 observations in (a) February 2015 and (b) August 2015. RMS, root mean square.

COM (0.22°C), or HYCOM (0.30°C). HYCOM has larger RMS errors than FIO-COM at 13 of the buoys (Figure 13a), and smaller CR values than either CMEMS or FIO-COM at most of the buoys (Figure 13b). The averaged RMS errors among these 19 buoys, with respect to FIO-COM, CMEMS, and HYCOM are 0.37°C, 0.23°C, and 0.42°C, and the corresponding averaged correlation coefficients are 93%, 96%, and 88%.

Figure 14 shows the SST comparisons at six selected TAO buoys located at (5°S, 125°W), (5°S, 140°W), (0°N, 125°W), (0°N, 140°W), (2°N, 125°W) and (2°N, 140°W). Climatological monthly mean SSTs obtained from

Table 3
Statistics of SST Comparisons Between FIO-COM, CMEMS, and HYCOM With all 19 TAO Buoys Located in Nino 3.4 Region in 2015

	FIO-COM				CMEMS				HYCOM			
TAO BUOY	ME (°C)	MAE (°C)	RMS (°C)	CR	ME (°C)	MAE (°C)	RMS (°C)	CR	ME (°C)	MAE (°C)	RMS (°C)	CR
(0°N, 125°W)	−0.52	0.54	0.64	0.93	0.22	0.25	0.31	0.98	0.32	0.40	0.50	0.93
(0°N, 140°W)	−0.42	0.42	0.48	0.95	0.09	0.14	0.17	0.98	0.22	0.29	0.39	0.90
(0°N, 155°W)	−0.21	0.28	0.34	0.97	0.09	0.14	0.18	0.99	0.39	0.43	0.56	0.94
(0°N, 170°W)	0.24	0.30	0.33	0.98	0.04	0.15	0.19	0.98	0.13	0.29	0.35	0.94
(2°N, 125°W)	−0.30	0.38	0.45	0.92	0.14	0.22	0.29	0.96	0.22	0.37	0.50	0.88
(2°N, 140°W)	−0.32	0.37	0.45	0.94	0.06	0.17	0.22	0.96	0.28	0.39	0.52	0.90
(2°N, 155°W)	−0.15	0.22	0.28	0.97	0.07	0.15	0.19	0.98	0.38	0.44	0.57	0.93
(2°N, 170°W)	0.30	0.34	0.42	0.93	0.19	0.24	0.30	0.95	0.19	0.32	0.43	0.89
(2°S, 125°W)	−0.19	0.28	0.33	0.96	0.11	0.15	0.19	0.99	0.11	0.26	0.35	0.93
(2°S, 140°W)	−0.27	0.35	0.41	0.96	0.05	0.10	0.13	0.99	0.17	0.24	0.32	0.95
(2°S, 155°W)	−0.22	0.28	0.33	0.97	0.05	0.16	0.20	0.98	0.25	0.33	0.44	0.92
(2°S, 170°W)	0.00	0.24	0.29	0.92	0.11	0.18	0.24	0.94	0.15	0.33	0.44	0.84
(5°N, 125°W)	0.16	0.31	0.39	0.92	0.12	0.23	0.29	0.90	0.27	0.39	0.56	0.75
(5°N, 155°W)	0.10	0.24	0.33	0.83	0.04	0.17	0.22	0.92	0.17	0.43	0.57	0.59
(5°N, 170°W)	0.34	0.35	0.37	0.92	−0.04	0.13	0.15	0.89	0.01	0.19	0.25	0.79
(5°S, 125°W)	−0.02	0.17	0.22	0.90	0.27	0.30	0.44	0.89	0.17	0.24	0.30	0.89
(5°S, 140°W)	−0.08	0.24	0.29	0.95	0.13	0.16	0.19	0.98	0.17	0.21	0.29	0.94
(5°S, 155°W)	−0.08	0.27	0.35	0.91	0.14	0.17	0.23	0.98	0.16	0.25	0.33	0.93
(5°S, 170°W)	0.00	0.20	0.25	0.79	0.11	0.15	0.20	0.91	0.20	0.28	0.39	0.80
Overall	−0.09	0.30	0.37	0.93	0.10	0.18	0.23	0.96	0.21	0.32	0.42	0.88

Abbreviations: CMEMS, copernicus marine and environment monitoring service; CR, correlation coefficient; FIO-COM, First Institute of Oceanography Coupled Ocean Model; HYCOM, hybrid isopycnal-sigma-pressure coordinate ocean model; MAE, mean absolute error; ME, mean error; RMS, root-mean-square error.

WOA13 can generally represent the SST variability in normal years, showing that the SSTs in the *Niño* 3.4 region usually keep rising from January to April and start to drop in May. However, SSTs obtained from the three analyses follow a similar rising pattern from January to April in 2015, then continued to suggest approximately steady temperatures, or to have slightly rising trends instead of decreasing from May until about December, which are consistent with the SST buoy observations. FIO-COM seems to underestimate the SSTs, whereas both CMEMS and HYCOM provide overestimations. HYCOM analysis shows high frequency SST fluctuations, which may be caused by high frequency atmospheric forcing. However, it is not possible for us to conduct the detailed related investigative studies, because only the assimilation products are available. At buoy (5°S, 125°W), CMEMS analysis shows larger values of SSTs than other datasets from August 2015 and later. A possible explanation is that overestimations in SST simulations in both CMEMS and HYCOM could be caused by insufficient mixing in the ocean models, which is a common challenge for nearly all ocean circulation models (Ezer, 2000; Huang et al., 2011; Huang & Qiao, 2010; Mellor, 2003). Improvements in mixing schemes in ocean models can lead to more realistic and reliable results. The application of the nonbreaking surface wave-induced mixing in FIO-COM can strengthen the vertical mixing and improve the simulations of MLD and SST (Qiao et al., 2004, 2010; Wu et al., 2015).

6. Discussion

The addition of the nonbreaking wave-induced mixing (B_v) term into the FIO-COM ocean model, brings a new perspective to the methodology to improve global assimilation products. Although the nonbreaking wave-induced mixing has been a controversy for decades, the continuing study of this term conducted in

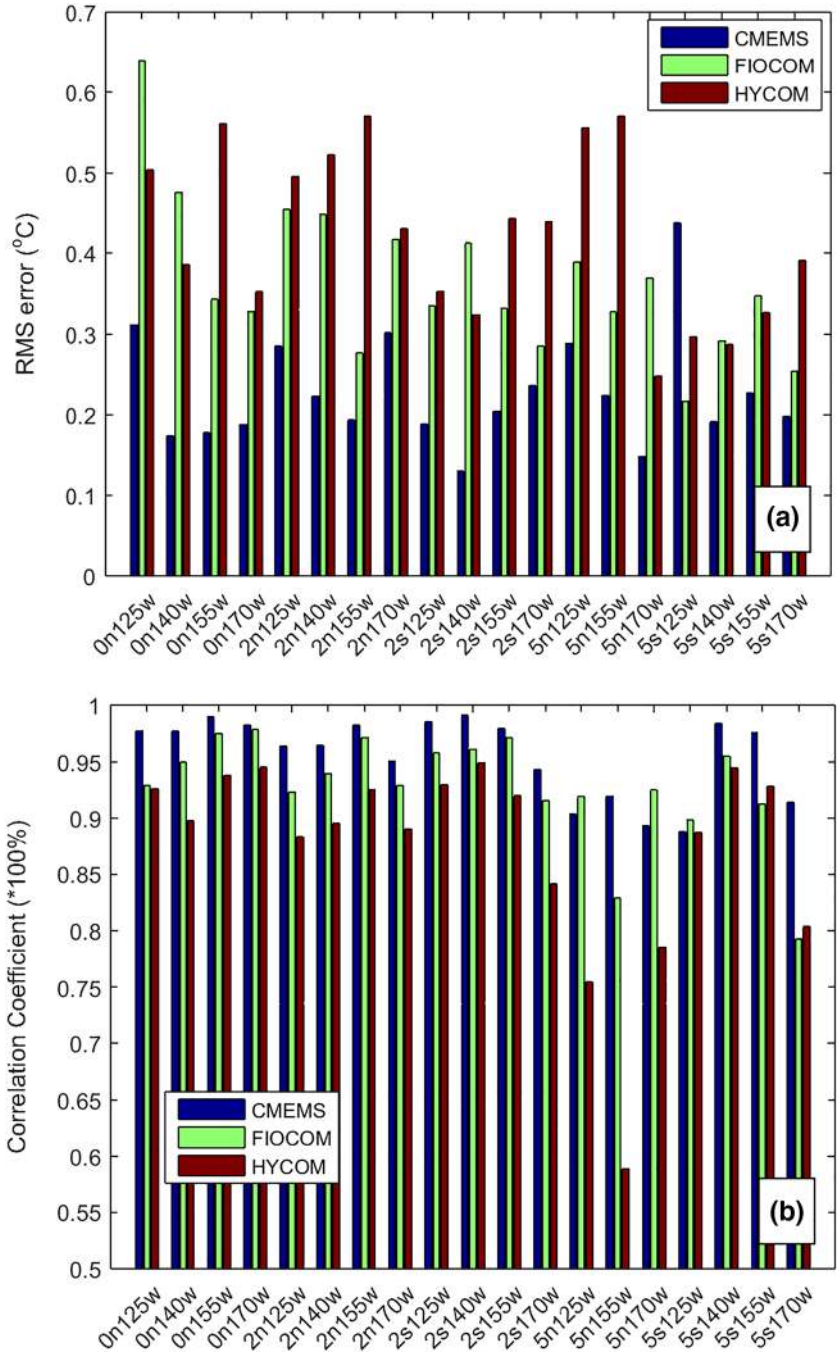

Figure 13. Statistics of comparisons from CMEMS, FIO-COM and HYCOM analysis datasets with the observations from all 19 TAO buoys located in the Niño 3.4 region based on the whole year SST time series in 2015 for (a) RMS errors; and (b) Correlation Coefficients. CMEMS, copernicus marine and environment monitoring service; FIO-COM, First Institute of Oceanography Coupled Ocean Model; HYCOM, hybrid isopycnal-sigma-pressure coordinate ocean model; RMS, root mean square; SST, sea surface temperature; TAO, tropical atmosphere ocean.

both theoretical and practical studies, has supported this approach. Applications of the B_v term in regional and global models, have resulted in improvements of their simulation ability (Pleskachevsky et al., 2011; Qiao et al., 2004; Shu et al., 2011; Wu et al., 2015). A quantification of the effect of the B_v term would involve sensitivity experiments, with and without the B_v term, using exactly the same ocean FIO-COM model system. That calculation is not achievable in the present study, due to the expense of the calculation. However,

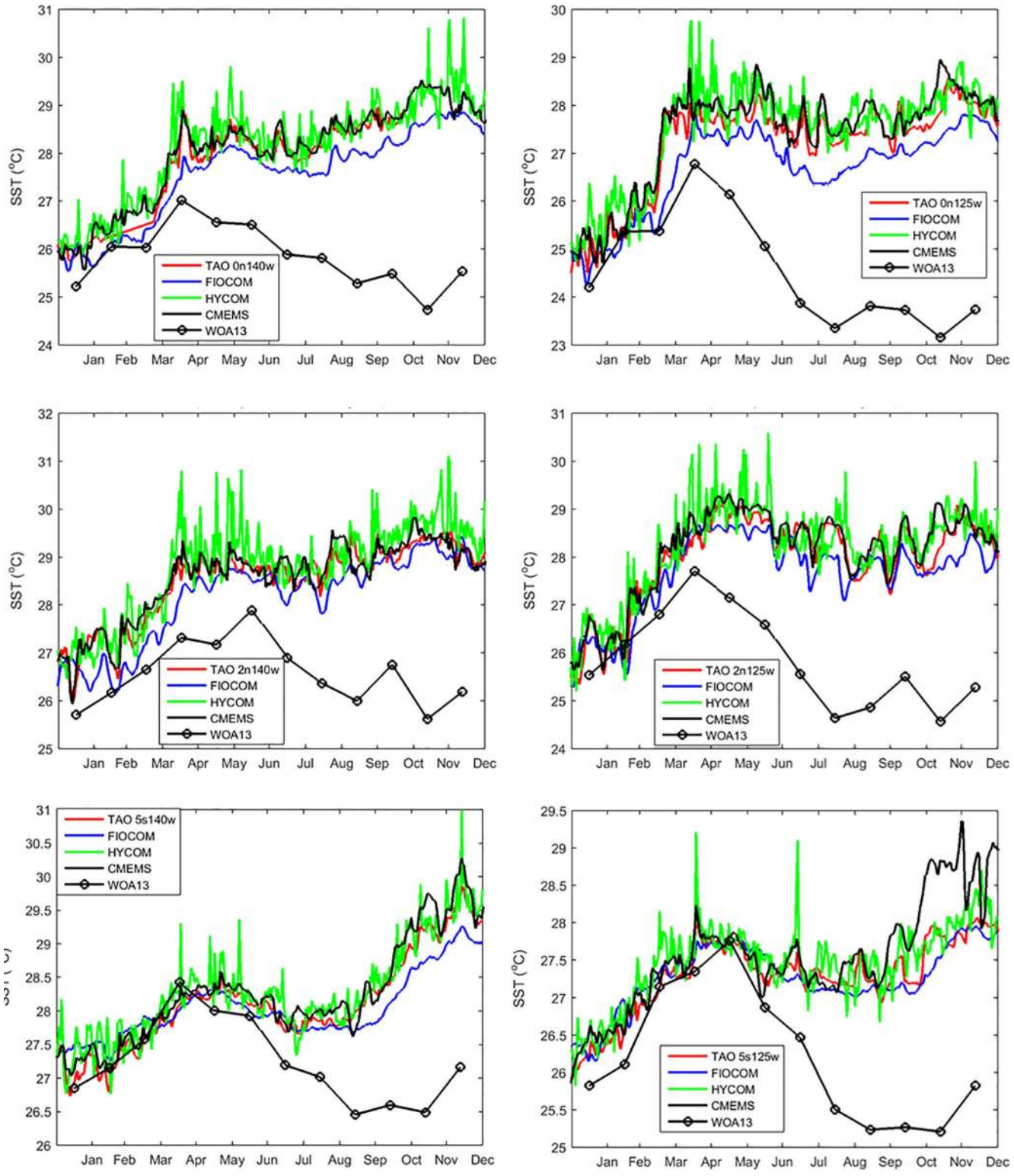

Figure 14. Comparisons of time series of SSTs between CMEMS, FIO-COM and HYCOM analysis data, with WOA13 climatological monthly SST, the SST observations from six selected TAO buoys located in Niño 3.4 region in 2015. CMEMS, copernicus marine and environment monitoring service; FIO-COM, First Institute of Oceanography Coupled Ocean Model; HYCOM, hybrid isopycnal-sigma-pressure coordinate ocean model; SST, sea surface temperature; TAO, tropical atmosphere ocean; WOA13, World Ocean Atlas 2013.

similar experiments have been introduced in the work of Qiao et al. (2016b), using four popular ocean models (MOM4, ROMS, POM, and NEMO) to conduct simulations, with and without the B_v term. The results reported by Qiao et al. (2016b) show that the simulated MLDs with B_v are dramatically improved in the Southern Ocean in January, providing solid evidence that the nonbreaking wave mixing plays a key role in the upper ocean.

Our exploration of the ocean model capabilities for the three analyses is restricted, because there are only the assimilation products available on the websites of CMEMS and HYCOM, and different assimilation schemes are used for each analysis. However, in follow-on presentations, we aim to deliver a new high-resolution global assimilation product, based on FIO-COM, and a first assessment of its performance is presented here. Thus, we have shown that the averaged RMS errors of FIO-COM analysis, for both the temperature and salinity profiles, in the region of focus (25°S-25°N, 180°W-180°E) in February and August of 2015 (Figure 12), indicate better performances, compared to that of HYCOM. This result is obtained even though fewer in situ observational datasets are assimilated into FIO-COM than into HYCOM; which suggests the advantage that wave-induced vertical mixing has for FIO-COM, especially in the interval from 50 to 150 m in the upper ocean. However, this hypothesis needs be further investigated in future work.

We obtained monthly mean simulation data from Mercator Ocean, corresponding to the CMEMS analysis, under an agreement for this specific validation work. As an example, we calculated the monthly mean MLD differences in both February and August of year 2015 between simulations (and analyses) and JAMSTEC data. Through Figures 15a and 15e, it may be seen that the Mercator simulation generally underestimates the MLDs especially in the tropical Pacific Ocean, whereas the FIO-COM simulation is a notable improvement on this problem (Figures 15b and 15f). This result may be attributed to the improvement of vertical mixing as discussed previously. However, the addition of the nonbreaking wave mixing also causes overestimation in the northern tropical oceans (Figure 15b) and in the southern tropical oceans (Figure 15f). By applying data assimilation, the performance of both analyses datasets is greatly improved (Figures 15c, 15d, 15g, and 15h), although there are small areas of underestimation from the Mercator analysis (or CMEMS analysis), and overestimation from the FIO-COM analysis.

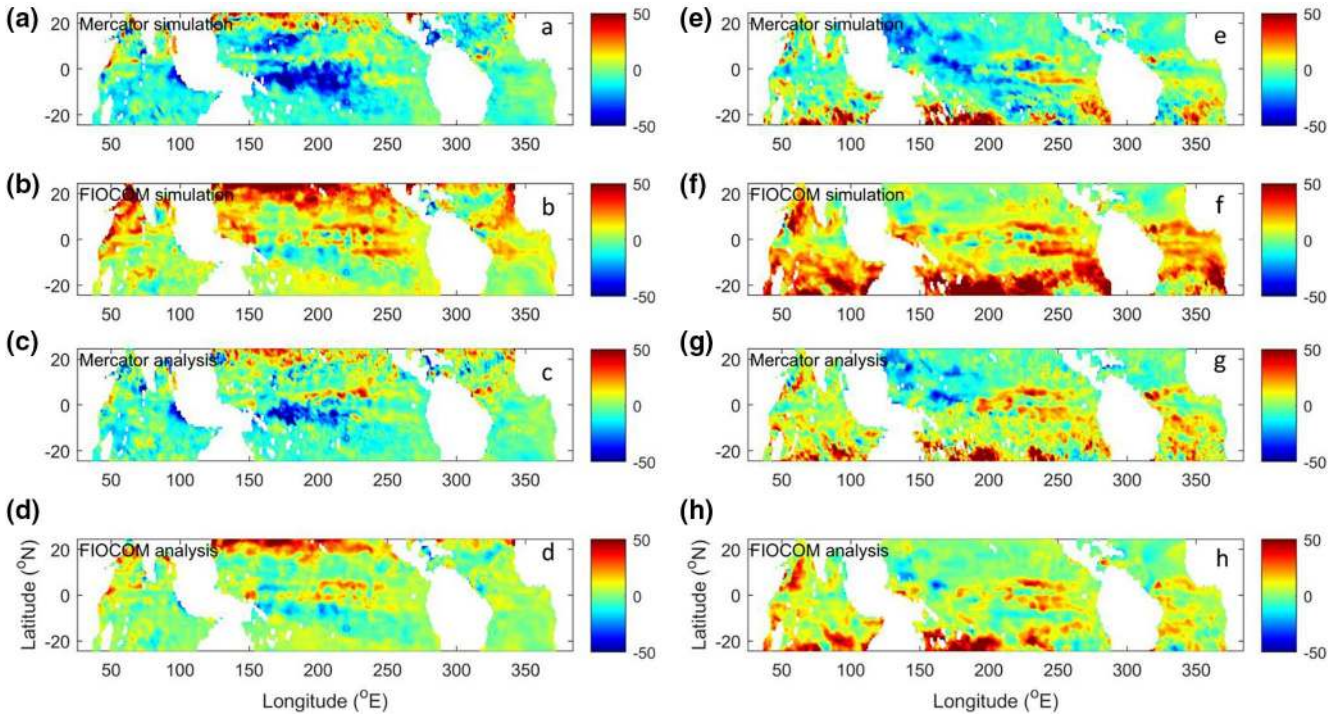

Figure 15. Monthly mean difference of MLD in February (left panel) and August of year 2015 (right panel), with respect to JAMSTEC, from (a and e) Mercator simulation; (b and f) FIO-COM simulation; (c and g) Mercator analysis; (d and h) FIO-COM analysis.

7. Summary

In this paper, the performance of the newly developed global high-resolution model, FIO-COM, is assessed, through intercomparisons with two other high-resolution global analyses, produced by HYCOM and CMEMS, against observations. The intercomparisons are conducted through: (1) examining the seasonal variations of MLDs estimated from analyses, (2) conducting quantitative assessment of daily T/S profiles, the 20°C isothermal depth and temperature at 5 m depth, compared to in situ T/S profiles, and (3) examining the model performance in simulating daily SSTs within the *Niño* 3.4 region during 2015 *El Niño*.

Both FIO-COM and CMEMS can accurately capture the large-scale MLD structures for all four seasons, whereas HYCOM underestimates the MLD in the southern tropical Pacific and tropical Atlantic Oceans in both summer and autumn. Moreover, FIO-COM analysis can capture more details of MLD seasonal variations in years 2014 and 2015, compared to JAMSTEC data. For example, the MLD more intensely deepens in the southern Arabian Sea as a result of stronger Indian Summer Monsoon; in the boreal autumn, the positive IOD strengthens the MLD deepening in the southern Indian Ocean with larger amplitudes compared to the springtime MLD shoaling.

In situ observations used in assimilations for HYCOM and CMEMS analyses (Argo, fixed and drifting buoys, CTDs, gliders and so on, https://www.godae-oceanview.org/science/ocean-forecasting-systems/assimilation-characteristics/), include the tropical buoy data, and so there is also a considerable overlap with EN4 temperature and salinity profiles which were used to validate the products. Compared with HYCOM and CMEMS analyses, the in situ observations assimilated into FIO-COM analysis only include Argo data. However, the intercomparisons between FIO-COM analysis and the other two analyses show a comparable performance, in the quantitative assessments of the 20°C isothermal depth, the temperature at 5 m depth, and T/S profiles, as well as the SST within the *Niño* 3.4 region in the tropical Pacific Ocean during the 2015 *El Niño* event. We hypothesize that this result might be attributed to the addition of the nonbreaking wave-induced mixing term in the ocean model, and the testing of this hypothesis requires further assimilation experiments.

In conclusion, the newly developed FIO-COM analysis provides an additional option for the oceanographic community in need of a high-resolution daily global ocean analysis data set, assessed and validated with reliable data. However, some improvements need to be done to the FIO-COM analysis in the future, including, but not limited to: (1) extension of the assessment of FIO-COM analysis to the global ocean, (2) provision of long-term operational outputs of the daily analysis data, which can be used to investigate ocean climate, and (3) assimilation of all available in situ temperature and salinity profiles into FIO-COM analysis to further improve its accuracy.

Acknowledgments
F. Qiao was supported by the National Natural Science Foundation of China under Grant 41821004 and the international cooperation project of Indo-Pacific ocean environment variation and air-sea interaction under Grant GASI-IPOVAI-05. G. Wang was supported by the National Key Research and Development Program of China Grant 2016YFC1401407 and 2016YFB0201100. Y. Sun and W. Perrie were supported by Canada's Aquatic Climate Change Adaptation Services Program, Ocean Frontier Institute and Marine Environmental Observation, Prediction and Response Network in this study. Y. Sun was supported by the ACCORD project (NE/R000123/1) at NOC during the revision of this manuscript. ACCORD was funded by the Natural Environment Research Council (NERC) and the Global Challenges Research Fund (GCRF) as part of a National Capability Official Development Assistance award.

Data Availability Statement

The CMEMS products used in this study are from E.U. Copernicus Marine Service Information, from http://marine.copernicus.eu/services-portfolio/access-to-products/?option=com_csw&view=details&product_id=GLOBAL_ANALYSIS_FORECAST_PHY_001_024. HYCOM analysis data are available at https://www.hycom.org/data/glbu0pt08.

References

Anderson, J. L. (2001). An ensemble adjustment Kalman filter for data assimilation. *Monthly Weather Review*, *129*, 2884–2903.
Bleck, R. (2002). An oceanic circulation model framed in hybrid isopycnic - cartesian coordinates. *Ocean Modelling*, *1*, 55–88.
Cabanes, C., Grouazel, A., Von Schuckmann, K., Hamon, M., Turpin, V., Coatanoan, C., et al. (2013). The CORA dataset: Validation and diagnostics of in-situ ocean temperature and salinity measurements. *Ocean Science*, *9*, 1–18. https://doi.org/10.5194/os-9-1-2013
Carton, J. A., Grodsky, S. A., & Liu, H. (2008). Variability of the oceanic mixed layer, 1960-2004. *Journal of Climate*, *21*, 1029–1047.
Chassignet, E. P., Hurlburt, H. E., Smedstad, O. M., Halliwell, G. R., Hogan, P. J., Wallcraft, A. J., et al. (2007). The HYCOM (hybrid Coordinate Ocean model) data assimilative system. *Journal of Marine Systems*, *65*, 60–83.
Chen, G., Han, W., Li, Y., McPhaden, M. J., Chen, J., Wang, W., et al. (2017). Strong intraseasonal variability of meridional currents near 5°N in the eastern Indian ocean: Characteristics and causes. *Journal of Physical Oceanography*, *47*, 979–998.
Chin, T. M., Vazquez-Cuervo, J., & Armstrong, E. M. (2017). A multi-scale high-resolution analysis of global sea surface temperature. *Remote Sensing of Environment*, *200*, 154–169.
Chiodi, A. M., & Harrison, D. E. (2017). Simulating ENSO SSTAs from TAO/TRITON winds: The impacts of 20 Years of buoy observations in the Pacific waveguide and comparison with analysis products. *Journal of Climate*, *30*, 1041–1059.

Cronin, M. F., & Kessler, W. S. (2002). Seasonal and interannual modulation of mixed layer variability at 0°N, 110°W. *Deep-Sea Research I*, *49*, 1–17.

Cummings, J. A. (2005). Operational multivariate ocean data assimilation. *Quarterly Journal of the Royal Meteorological Society, Part C*, *131*(613), 3583–3604.

Cummings, J. A., & Smedstad, O. M. (2013). Variational data analysis for the global ocean. In S. K. Park & L. Xu (Eds.), *Data assimilation for atmospheric, oceanic and hydrologic applications* (Vol. II). Springer-Verlag Berlin Heidelberg. https://doi.org/10.1007/978-3-642-35088-7_13

Cummings, J. A., & Smedstad, O. M. (2014). Ocean data impacts in global HYCOM. *Journal of Atmospheric and Oceanic Technology*, *31*, 1771–1791.

Da-Allada, C. Y., Jouanno, J., Gaillard, F., Kolodziejczyk, N., Maes, C., Reul, N., et al. (2017). Importance of the Equatorial Undercurrent on the sea surface salinity in the eastern equatorial Atlantic in boreal spring. *Journal of Geophysical Research: Oceans*, *122*, 521–538. https://doi.org/10.1002/2016JC012342

de Boyer Montégut, C., Madec, G., Fischer, A. S., Lazar, A., & Iudicone, D. (2004). Mixed layer depth over the global ocean: An examination of profile data and a profile-based climatology. *Journal of Geophysical Research*, *109*, C12003. https://doi.org/10.1029/2004JC002378

Dickey, T. D. (2003). Emerging ocean observations for interdisciplinary data assimilation systems. *Journal of Marine Systems*, *40–41*, 5–48.

Ezer, T. (2000). On the seasonal mixed layer simulated by a basin-scale ocean model and the Mellor-Yamada turbulence scheme. *Journal of Geophysical Research*, *105*, 16843–16855.

Fan, Y., & Griffies, S. M. (2014). Impacts of parameterized langmuir turbulence and nonbreaking wave mixing in global climate simulations. *Journal of Climate*, *27*, 4752–4775.

Foltz, G. R., Grodsky, S. A., Carton, J. A., & McPhaden, M. J. (2003). Seasonal mixed layer heat budget of the tropical Atlantic Ocean. *Journal of Geophysical Research*, *108*(C5), 3146. https://doi.org/10.1029/2002JC001584

Girard-Ardhuin, F., & Ezraty, R. (2012). Enhanced Arctic sea ice drift estimation merging radiometer and scatterometer data. *IEEE Transactions on Geoscience and Remote Sensing*, *50*(7), 2639–2648. https://doi.org/10.1109/TGRS.2012.2184124

Good, S. A., Martin, M. J., & Rayner, N. A. (2013). EN4: Quality controlled ocean temperature and salinity profiles and monthly objective analyses with uncertainty estimates. *Journal of Geophysical Research: Oceans*, *118*, 6704–6716. https://doi.org/10.1002/2013JC009067

Griffies, S. M. (2012). *Elements of the modular ocean model (MOM) (2012 release with updates), GFDL ocean group technical report No. 7, NOAA/Geophysical Fluid Dynamics Laboratory*, p. 632 + xiii.

Griffies, S. M., Biastoch, A., Böning, C., Bryan, F., Danabasoglu, G., Chassignet, E. P., et al. (2009). Coordinated ocean-ice reference experiments (COREs). *Ocean Modelling*, *26*, 1–46.

Grunseich, G., Subrahmanyam, B., Murty, V. S. N., & Giese, B. S. (2011). Sea surface salinity variability during the Indian Ocean Dipole and ENSO events in the tropical Indian Ocean. *Journal of Geophysical Research*, *116*, C11013. https://doi.org/10.1029/2011JC007456

Halliwell, G. R. (2004). Evaluation of vertical coordinate and vertical mixing algorithms in the hybrid coordinate ocean model (HYCOM). *Ocean Modelling*, *7*, 285–322.

Halliwell, G., Bleck, R., & Chassignet, E. (1998). *Atlantic Ocean simulations performed using a new hybrid-coordinate ocean model*. EOS, Trans. AGU, Fall 1998 AGU meeting.

Hosoda, S., Ohira, T., & Nakamura, T. (2008). A monthly mean dataset of global oceanic temperature and salinity derived from Argo float observations. *JAMSTEC Report of Research and Development*, *8*, 47–59.

Huang, C., & Qiao, F. (2010). Wave-breaking interaction and its induced mixing in the upper ocean. *Journal of Geophysical Research*, *115*, C04026. https://doi.org/10.1029/2009JC005853

Huang, C., Qiao, F., Song, Z., & Ezer, T. (2011). Improving simulations of the upper ocean by inclusion of surface waves in the Mellor-Yamada turbulence scheme. *Journal of Geophysical Research*, *116*, C01007. https://doi.org/10.1029/2010JC006320

Ignatov, A., Zhou, X., Petrenko, B., Liang, X., Kihai, Y., Dash, P., et al. (2016). AVHRR GAC SST analysis version 1 (RAN1). *Remote Sens*, *8*, 315. https://doi.org/10.3390/rs8040315

Jayne, S. R., & St. Laurent, L. C. (2001). Parameterizing tidal dissipation over rough topography. *Geophysical Research Letters*, *28*(5), 811–814.

Kara, A. B., Rochford, P. A., & Hurlburt, H. E. (2000). An optimal definition for ocean mixed layer depth. *Journal of Geophysical Research*, *105*, 16803–16821.

Kara, A. B., Rochford, P. A., & Hurlburt, H. E. (2003). Mixed layer depth variability over the global ocean. *Journal of Geophysical Research*, *108*(C3), 3079. https://doi.org/10.1029/2000JC000736

Kara, A. B., Wallcraft, A. J., & Bourassa, M. A. (2008a). Air-sea stability effects on the 10 m winds over the global ocean: Evaluations of air-sea flux algorithms. *Journal of Geophysical Research*, *113*, C04009. https://doi.org/10.1029/2007JC0044324

Kara, A. B., Wallcraft, A. J., Martin, P. J., & Chassignet, E. P. (2008b). Performance of mixed layer models in simulating SST in the equatorial Pacific Ocean. *Journal of Geophysical Research*, *113*, C02020. https://doi.org/10.1029/2007JC004250

Keerthi, M. G., Lengaigne, M., Vialard, J., de Boyer Montégut, C., & Muraleedharan, P. M. (2013). Interannual variability of the Tropical Indian Ocean mixed layer depth. *Climate Dynamics*, *40*, 743–759. https://doi.org/10.1007/s00382-012-1295-2

Kirtman, B. P., Bitz, C., Bryan, F., Collins, W., Dennis, J., Hearn, N., et al. (2012). Impact of ocean model resolution on CCSM climate simulations. *Climate Dynamics*, *39*, 1303–1328.

Large, W., & Yeager, S. (2004). *Diurnal to decadal global forcing for Ocean and sea-ice models: The data sets and flux climatologies*. NCAR Technical Note: NCAR/TN-460+STR CGD Division of the National Center for Atmospheric Research.

Lee, E., Noh, Y., Liu, B., & Yeh, S. W. (2015). Seasonal variation of the upper ocean responding to surface heating in the North Pacific. *Journal of Geophysical Research: Oceans*, *120*, 5631–5647. https://doi.org/10.1002/2015JC010800

Lellouche, J. M., Le Galloudec, O., Drévillon, M., Régnier, C., Greiner, E., Garric, G., et al. (2013). Evaluation of global monitoring and forecasting systems at Mercator Océan. *Ocean Science*, *9*, 57–81.

Li, J., Liang, C., Tang, Y., Dong, C., Chen, D., Liu, X., et al. (2016). A new dipole index of the salinity anomalies of the tropical Indian Ocean. *Scientific Reports*, *6*, 24260. https://doi.org/10.1038/srep24260

Locarnini, R. A., Mishonov, A. V., Antonov, J. I., Boyer, T. P., Garcia, H. E., Baranova, O. K., et al. (2013). In S. Levitus (Ed.), *World ocean atlas 2013, volume 1: Temperature* (A. Mishonov Technical Ed., p. 40). NOAA Atlas NESDIS 73.

Lü, X., Qiao, F., Wang, G., Xia, C., & Yuan, Y. (2008). Upwelling off the west coast of Hainan Island in summer: Its detection and mechanisms. *Geophysical Research Letters*, *35*, L02604. https://doi.org/10.1029/2007GL032440

Madec, G., & the NEMO team (2008). NEMO ocean engine. Note du Pôle de modélisation, Institut Pierre-Simon Laplace (IPSL), France, No. 27. ISSN, 1288–1619.

Madec, G., & Imbard, M. (1996). A global ocean mesh to overcome the North Pole singularity. *Climate Dynamics*, *12*, 381–388.

Mellor, G. (2003). The three-dimensional current and surface wave equations. *Journal of Physical Oceanography*, *33*, 1978–1989.
Monterey, G., & Levitus, S. (1997). *Seasonal variability of mixed layer depth for the World Ocean*. NOAA Atlas NESDIS 14. Silver Spring, MD: National Oceanic and Atmospheric Administration.
Pleskachevsky, A., Dobrynin, M., Babanin, A. V., Günther, H., & Stanev, E. (2011). Turbulent mixing due to surface waves indicated by remote sensing of suspended particulate matter and its implementation into coupled modeling of waves, turbulence, and circulation. *Journal of Physical Oceanography*, *41*, 708–724. https://doi.org/10.1175/2010JPO4328.1
Qiao, F., Yang, Y., & Xia, C. (2008). The role of surface waves in the ocean mixed layer. *Acta Oceanologica Sinica*, *27*(3), 30–37.
Qiao, F., Yuan, Y., Deng, J., Dai, D., & Song, Z. (2016b). Wave-turbulence interaction-induced vertical mixing and its effects in ocean and climate models. *Philosophical Transactions of the Royal Society A*, *374*, 20150201. https://doi.org/10.1098/rsta.2015.0201
Qiao, F., Yuan, Y., Ezer, T., Xia, C., Yang, Y., Lü, X., et al. (2010). A three-dimensional surface wave-ocean circulation coupled model and its initial testing. *Ocean Dynamics*, *60*(5), 1339–1355. https://doi.org/10.1007/s10236-010-0326-y
Qiao, F., Yuan, Y., Yang, Y., Zheng, Q., Xia, C., & Ma, J. (2004). Wave-induced mixing in the upper ocean: Distribution and application to a global ocean circulation model. *Geophysical Research Letters*, *31*, L11303. https://doi.org/10.1029/2004GL019824
Qiao, F., Zhao, W., Yin, X., Huang, X., Liu, X., Shu, Q., et al. (2016a). *A highly effective global surface wave numerical simulation with ultra-high resolution*. In Proceedings of the international conference for high performance computing, networking, storage and analysis (SC16). Piscataway, NJ: IEEE Press. Article 5, 46-56, ISBN 978-1-4673-8815-3. Retrieved From http://dl.acm.org/citation.cfm?id=3014904.3014911
Rugg, A., Foltz, G. R., & Perez, R. C. (2016). Role of mixed layer dynamics in tropical North Atlantic interannual sea surface temperature variability. *Journal of Climate*, *29*, 8083–8101.
Saji, N. H., Goswami, B. N., Vinayachandran, P. N., & Yamagata, T. (1999). A dipole mode in the tropical Indian Ocean. *Nature*, *401*, 360–363.
Scaife, A. A., Copsey, D., Gordon, C., Harris, C., Hinton, T., Keeley, S., et al. (2011). Improved Atlantic winter blocking in a climate model. *Geophysical Research Letters*, *38*, L23703. https://doi.org/10.1029/2011GL049573
Shu, Q., Qiao, F., Song, Z., Xia, C., & Yang, Y. (2011). Improvement of MOM4 by including surface wave-induced vertical mixing. *Ocean Modelling*, *40*(1), 42–51.
Soufflet, Y., Marchesiello, P., Lenarié, F., Jouanno, J., Capet, X., Debreu, L., & Benshila, R. (2016). On effective resolution in ocean models. *Ocean Modelling*, *98*, 36–50.
Subrahmanyam, B., Murty, V. S. N., & Heffner, D. M. (2011). Sea surface salinity variability in the tropical Indian Ocean. *Remote Sensing of Environment*, *115*, 944–956.
Taylor, K. E. (2001). Summarizing multiple aspects of model performance in a single diagram. *Journal of Geophysical Research*, *106*, 7183–7192.
Thompson, B., Gnanaseelan, C., & Salvekar, P. S. (2006). Variability in the Indian Ocean circulation and salinity and its impact on SST anomalies during dipole events. *Journal of Marine Research*, *64*, 853–880.
Toyoda, T., Fujii, Y., Kuragano, T., Kamachi, M., Ishikawa, Y., Masuda, S., et al. (2017). Intercomparison and validation of the mixed layer depth fields of global ocean syntheses. *Climate Dynamics, 49*, 753–773. https://doi.org/10.1007/s00382-015-2637-7
Wang, B., Wu, R., & Lau, K. M. (2001). Interannual variability of the Asian summer monsoon: Contrasts between the Indian and the western North Pacific-east Asian monsoon. *Journal of Climate*, *14*, 4073–4090.
Winton, M. (2000). A reformulated three-layer sea ice model. *Journal of Atmospheric and Oceanic Technology*, *17*, 525–531.
Wu, L., Rutgersson, A., & Sahlée, E. (2015). Upper-ocean mixing due to surface gravity waves. *Journal of Geophysical Research: Oceans*, *120*(12), 8210–8228. https://doi.org/10.1002/2015JC011329
Xiao, B., Qiao, F., & Shu, Q. (2016). The performance of a Z-level ocean model in modeling global tide. *Acta Oceanologica Sinica*, *35*(11), 35–43. https://doi.org/10.1007/s13131-016-0884-z
Yeh, S.-W., Yim, B. Y., Noh, Y., & Dewitte, B. (2009). Changes in mixed layer depth under climate change projections in two CGGMs. *Climate Dynamics*, *33*, 199–213.
Yin, X., Qiao, F., & Shu, Q. (2011). Using ensemble adjustment Kalman filter to assimilate Argo profiles in a global OGCM. *Ocean Dynamics*, *61*, 1017–1031. https://doi.org/10.1007/s10236-011-0419-2
Yin, X., Qiao, F., Yang, Y., Xia, C., & Chen, X. (2012). Argo data assimilation in ocean general circulation model of Northwest Pacific Ocean. *Ocean Dynamics*, *62*(7), 1059–1071. https://doi.org/10.1007/s10236-012-0549-1